Biophysical Journal
Article

Biophysical Society

Effects of microRNA-mediated negative feedback on gene expression noise

Raunak Adhikary,[1] Arnab Roy,[1] Mohit Kumar Jolly,[2] and Dipjyoti Das[1,*]
[1]Department of Biological Sciences, Indian Institute of Science Education And Research Kolkata Mohanpur, Nadia, West Bengal, India and [2]Centre for BioSystems Science and Engineering, Indian Institute of Science, Bengaluru, India

ABSTRACT MicroRNAs (miRNAs) are small noncoding RNAs that regulate gene expression post-transcriptionally in eukaryotes by binding with target mRNAs and preventing translation. miRNA-mediated feedback motifs are ubiquitous in various genetic networks that control cellular decision making. A key question is how such a feedback mechanism may affect gene expression noise. To answer this, we have developed a mathematical model to study the effects of a miRNA-dependent negative-feedback loop on mean expression and noise in target mRNAs. Combining analytics and simulations, we show the existence of an expression threshold demarcating repressed and expressed regimes in agreement with earlier studies. The steady-state mRNA distributions are bimodal near the threshold, where copy numbers of mRNAs and miRNAs exhibit enhanced anticorrelated fluctuations. Moreover, variation of negative-feedback strength shifts the threshold locations and modulates the noise profiles. Notably, the miRNA-mRNA binding affinity and feedback strength collectively shape the bimodality. We also compare our model with a direct auto-repression motif, where a gene produces its own repressor. Auto-repression fails to produce bimodal mRNA distributions as found in miRNA-based indirect repression, suggesting the crucial role of miRNAs in creating phenotypic diversity. Together, we demonstrate how miRNA-dependent negative feedback modifies the expression threshold and leads to a broader parameter regime of bimodality compared to the no-feedback case.

SIGNIFICANCE How post-transcriptional regulation affects gene expression noise is an important open question. Small noncoding RNAs, called microRNAs (miRNAs), bind to mRNAs, preventing translation in eukaryotes. The mRNA and miRNA-producing genes are often coupled via feedback. Here, we focused on a miRNA-mediated negative-feedback loop to theoretically study the mean and variance of target mRNAs. With increasing miRNA synthesis, we found that the mean mRNA shifts from high to low levels beyond a threshold. The negative-feedback strength and the mRNA-miRNA catalytic interaction collectively modulate these thresholds, where mRNA distributions display bimodality with enhanced number fluctuations. Further, we compared an auto-repression motif with the miRNA-mediated repression and found that only the latter can produce bimodality, signifying its role in phenotypic heterogeneity.

INTRODUCTION

To survive, cells actively regulate the processes of transcription and translation in response to environmental cues (1). However, since biological molecules are present in low numbers in a cell and due to the heterogeneity of environmental factors, large cell-to-cell fluctuations can exist in mRNA and protein copy numbers. Thus, transcription and translation are inherently stochastic processes leading to the heterogeneity of gene products in genetically identical cell populations; this phenomenon is known as gene expression noise (2–5). Understanding how gene expression noise is regulated has emerged as an important research area in molecular biology (5–10).

Genes are mainly regulated via the binding and unbinding of diverse transcription factors (TFs) at specific sites close to the promoter. Such control on the promoter architecture through TF binding can modulate expression noise, as found in theoretical studies (5,11–16) and experiments (17–22). Phenotypic consequences of expression variability were also investigated, and it was found that gene expression noise can control cell fate switching and have survival benefits in varying environments (23–26).

Post-transcriptional regulation by short noncoding RNAs is another common mechanism for controlling

Submitted February 24, 2023, and accepted for publication September 28, 2023.

*Correspondence: dipjyoti.das@iiserkol.ac.in

Editor: Ramon Grima.
https://doi.org/10.1016/j.bpj.2023.09.019

gene expression in both prokaryotes and eukaryotes. For instance, noncoding small RNAs (sRNAs) in bacteria bind with target mRNAs to facilitate mRNA degradation (27–32). Similarly, eukaryotic microRNAs (miRNAs) are about 22-nucleotide-long noncoding RNAs that interact with mRNAs in a sequence-dependent manner. After maturing into RNA-induced silencing complexes (RISCs), miRNAs can bind to the 3′ UTR of the target mRNAs and then either degrade the transcript or inhibit their translation (1,33). Such post-transcriptional control by miRNAs affects various biological processes, including animal development, stabilization of gene expression as a stress response, and inhibition of cancer metastasis (34–38).

Previous quantitative studies have suggested that the interplay between mRNAs and miRNAs (or sRNAs) occurs via a molecular titration-like mechanism (30,39). However, the mode of interaction between miRNAs and mRNAs is still debated. Some studies advocate an almost catalytic interaction (40,41), and some suggest stoichiometric interaction (42–44). During catalytic interaction, miRNAs recycle back, maintaining a pool (33,45,46), whereas miRNAs and mRNAs could destroy each other through stoichiometric interaction. On the other hand, prokaryotic sRNAs mainly act stoichiometrically on their target mRNAs (47,48). Nevertheless, both eukaryotic miRNA and prokaryotic sRNA can produce a threshold-like behavior at the mean expression level, with a sharp demarcation of low- and high-expression regimes, due to a competitive titration between miRNAs (or sRNAs) and their targets (30,31,39,49). Although some theoretical studies have focused on miRNA-mediated gene expression noise (46,49–51), there are still some differences in opinions. For instance, one study (52) claimed that catalytic interaction reduces gene expression noise compared to stoichiometric interaction involving miRNAs, but another study (49) asserted that both stoichiometric and catalytic interactions produce qualitatively similar noise in certain parameter regimes.

An exciting aspect of miRNA-mediated regulation is that one class of miRNAs can affect many distinct genes, leading to the competing endogenous RNA (ceRNA) hypothesis, which suggests regulating the expression of one gene by affecting the transcription of another gene that shares the same pool of miRNAs. Theoretical and experimental works based on the ceRNA hypothesis have shown that multiple target mRNAs influence each other nonlinearly through a common pool of miRNAs, producing high variability in expression (33,45,53–55). As reported in sRNA-dependent bimodal gene expression (56), miRNA-dependent bimodal expression in ceRNA networks was also predicted theoretically (33,49) and later shown in experiments (45,46).

Notably, miRNA-dependent feedback motifs are ubiquitous in regulatory networks (57), which dictate diverse physiological and developmental processes, including cell cycle control (58), cancer cell proliferation, chemoresistance, angiogenesis (59–61), and host-HIV interaction (62). Feedback involving miRNAs establishes a cross-talk between post-transcriptional and transcriptional layers to precisely regulate some transitions of biological states. For example, the network controlling epithelial-mesenchymal transition during cancer progression involves miRNA-mediated feedback loops. (63,64). Another well-known example is the differentiation of precursor cells into dopamine neurons in the midbrain, which is governed by a negative-feedback loop involving the miRNA, miR-133b, and the TF, *pitx3* (65).

Despite mounting evidence that miRNAs are critical downregulators of gene expression, the theoretical understanding of miRNA-based feedback loops in regulating gene expression noise is still incomplete. Several theoretical studies have focused on the miRNA-based feedback loops, albeit mainly from a deterministic standpoint focusing on the mean level (reviewed in (66)). Among different feedback motifs, those involving negative feedback are of particular interest because of their capacity to buffer gene expression noise (66–68). Using a deterministic mean-field approach, Zhou et al. have studied a miRNA-based single-negative-feedback loop (SNFL), where a TF promotes the expression of a miRNA that, in turn, inhibits the TF expression (69). Another study focused on a similar SNFL to investigate both the mean and noise of expression, but the interactions between the miRNA-producing gene and TFs were modeled in a coarse-grained way (70).

In this paper, we developed a detailed model of the miRNA-mediated SNFL and investigated the properties of mean and variance of expression in the steady state. We found that the steady-state mean mRNA shows a threshold-linear behavior; i.e., the mean is almost zero below a threshold transcription rate, and the mean increases almost linearly above the threshold. This observation agrees with earlier studies without any feedback (39,49). Such a threshold stems from a competitive titration between miRNAs and mRNAs, and the threshold point corresponds to the situation when the numbers of mRNAs and miRNAs are comparable. Our mean-field calculation also provided an analytical expression for the threshold, which shows that the threshold point crucially depends on miRNA's catalytic interaction and feedback strength. Notably, the noise in mRNA copy numbers also peaked in the threshold's vicinity, suggesting the genetic motif's high sensitivity at this region. We also found bimodal mRNA distributions near the threshold, unlike a similar theoretical study on miRNA-mediated negative feedback (70). Such bimodal distributions correspond to large anticorrelated fluctuation in miRNA and mRNA numbers, suggesting stochastic switching of mRNAs between two states: miRNA bound (repressing the target mRNAs) and miRNA unbound (expressing the mRNAs).

Finally, we compared the outputs of a miRNA-mediated negative-feedback loop with a negative auto-regulatory loop since auto-regulatory motifs are essential components in many genetic networks often seen in various biological contexts (71–73). An auto-regulatory motif, where a protein expressed from a gene acts as a TF for the same gene, can be either positive or negative, depending on whether the TF enhances or suppresses its own expression. A positive auto-regulation produces bi-stable expression, and subsequent bimodal protein distribution, enhancing the expression noise (71,74–78), whereas negative auto-regulation can suppress noise (79–82). However, some recent theoretical studies created a difference in opinion using different assumptions and showed that negative auto-regulation can also enhance noise in certain situations (83,84). These contradictory results were resolved by a recent study (85) where the authors decomposed the total noise into the feedback-free noise and the feedback coefficient and showed that positive feedback enhances the feedback coefficient (rather than the total noise), whereas negative feedback reduces it.

When we compared our model of miRNA-based negative feedback with an auto-repression, at first glance, both circuits exhibited qualitatively similar behavior of the mean and noise as functions of respective feedback strengths. However, we found that negative feedback involving miRNAs produces bimodal mRNA distribution by amplifying noise, but auto-repression leads to only bell-shaped mRNA distributions. Our study thus highlights the importance of miRNA-based negative feedback in producing phenotypic diversity.

Model

We adapted a published model (33) of miRNA-mRNA interaction (without any feedback) to describe the miRNA-mediated negative-feedback loop (see Fig. 1). In the model, the mRNA molecules are synthesized from an mRNA-coding gene at a constant rate k_r, and then protein molecules are produced from the mRNAs at a rate k_p. The mRNAs and proteins degrade with rates g_r and g_p, respectively. The translation of mRNAs into proteins is inhibited post-transcriptionally by the miRNA molecules produced from a miRNA-coding gene at a basal rate k_s^0. The miRNAs degrade at a rate g_s. The proteins can activate the miRNA-coding gene and increase the miRNA synthesis rate, establishing a negative feedback on gene expression. Thus, the miRNA-coding gene can be in two distinct states based on the miRNA synthesis rate: miRNAs are produced either at a basal rate (k_s^0) or at an enhanced rate ($k_s > k_s^0$) (see Fig. 1). These states are termed "off" (basal) and "on" (enhanced), respectively. The protein binds at a rate k_{act} to the miRNA-coding gene, making it switch from off (basal) to on (enhanced) state. Thus, k_{act} is termed the activation rate of the miRNA

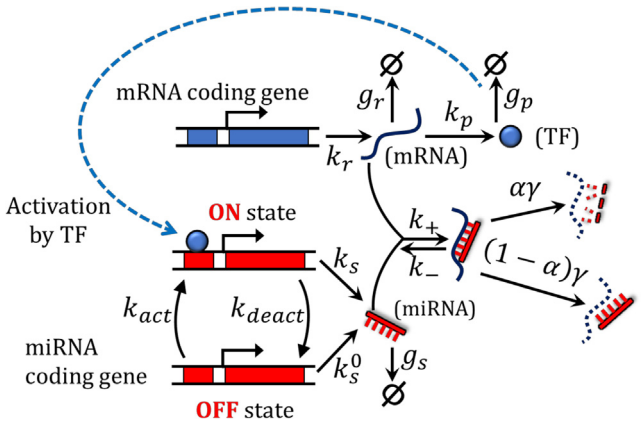

FIGURE 1 Schematic diagram of miRNA-mediated negative feedback showing various kinetic processes with corresponding rates (see model and Table 1). The miRNAs bind with the target mRNAs to form miRNA-mRNA complexes. The complexes degrade with a rate $\alpha\gamma$, or the miRNAs act catalytically, degrading only the mRNAs (rate $(1-\alpha)\gamma$). The parameter α ($0 \le \alpha \le 1$; called catalyticity parameter) determines the fraction of miRNAs that are degraded when they are bound to mRNAs. The mRNAs produce a transcription factor (TF) that activates a miRNA-coding gene and enhances its transcription rate more than the basal rate (in general, $k_s > k_s^0$). Thus, the miRNA-coding gene toggles between on (activated) and off (basal) states. Here, $\beta = k_{act}/k_{deact}$ can be considered as the feedback strength, whereas $g = k_+\gamma/(k_- + \gamma)$ is an effective association rate between miRNAs and mRNAs. To see this figure in color, go online.

gene. On the other hand, the switch from the on to off state occurs when the bound protein dissociates from the miRNA-coding gene (rate, k_{deact}). Note that the nondimensional ratio $\beta = k_{act}/k_{deact}$ can be considered as the negative-feedback strength. Since the post-transcriptional regulation of mRNAs takes place via direct association and dissociation between mRNAs and miRNAs, we consider the binding (rate k_+) and unbinding (rate k_-) processes between an mRNA and a miRNA, thereby forming an mRNA-miRNA complex. The mRNA-miRNA complex may disintegrate in two ways: 1) either the complex fully degrades at a rate $\alpha\gamma$, simultaneously destroying both the mRNA and miRNA molecules, or 2) only the bound mRNA is degraded (with a rate $(1-\alpha)\gamma$) and the miRNA is recycled back. Here, γ denote a complex disintegration rate, and α ($0 \le \alpha \le 1$) is the catalyticity parameter. Note that α determines the fraction of miRNAs recycled after dissociating from their target mRNAs.

Based on the model, we described the time evolution of four stochastic integer-valued variables, namely the instantaneous numbers of mRNAs, proteins, miRNAs, and mRNA-miRNA complexes (denoted by $r(t)$, $p(t)$, $s(t)$, and $c(t)$, respectively). Using the framework of stochastic processes, we write down below the Master equation governing the joint probability distribution, $P_{r,p,s,c}(t)$, defined as the probability of observing $r, p, s,$ and c number of mRNAs, proteins, miRNAs, and complexes, respectively, at a time t.

$$\begin{aligned}\frac{\partial P_{r,p,s,c}}{\partial t} &= k_r\left[P_{r-1,p,s,c} - P_{r,p,s,c}\right] + g_r\left[(r+1)P_{r+1,p,s,c} - rP_{r,p,s,c}\right] \\ &+k_p\left[rP_{r,p-1,s,c} - rP_{r,p,s,c}\right] + g_p\left[(p+1)P_{r,p+1,s,c} - pP_{r,p,s,c}\right] \\ &+k_{deact}\left[P^{ON}_{r,p-1,s,c} - P^{ON}_{r,p,s,c}\right] + k_{act}\left[(p+1)P^{OFF}_{r,p+1,s,c} - pP^{OFF}_{r,p,s,c}\right] \\ &+k_s^0\left[P^{OFF}_{r,p,s-1,c} - P^{OFF}_{r,p,s,c}\right] + k_s\left[P^{ON}_{r,p,s-1,c} - P^{ON}_{r,p,s,c}\right] + g_s\left[(s+1)P_{r,p,s+1,c} - sP_{r,p,s,c}\right] \\ &+k_+\left[(r+1)(s+1)P_{r+1,p,s+1,c-1} - rsP_{r,p,s,c}\right] + k_-\left[(c+1)P_{r-1,p,s-1,c+1} - cP_{r,p,s,c}\right] \\ &+\alpha\gamma\left[(c+1)P_{r,p,s,c+1} - cP_{r,p,s,c}\right] + (1-\alpha)\gamma\left[(c+1)P_{r,p,s-1,c+1} - cP_{r,p,s,c}\right]\end{aligned} \tag{1}$$

The Master equation (Eq. 1) is constructed by accounting for the "gain" and "loss" terms corresponding to all possible changes in the model variables (r, p, s, or c). Here, $P_{r,p,s,c}(t)$ is the joint probability distribution irrespective of the miRNA-gene state (on or off), and hence it can be broken into two parts: $P_{r,p,s,c}(t) = P^{OFF}_{r,p,s,c}(t) + P^{ON}_{r,p,s,c}(t)$ (corresponding to each state; see Eq. S1.1–S1.3 in Supporting material).

We obtained the time-evolution equations for means and variances of our variables (i.e., first- and second-order moments) from the Master equation described above (see Eq. S2.1–S2.29 in Supporting material). However, the moment equations do not close themselves since each equation contains the next higher-order moment. Due to this challenge, we obtained approximate equations for the means and variances (by neglecting higher-order moments) that can be tackled analytically (Eq. S3.1–S3.5 and Eq. S6.1–S6.20). Alternatively, we performed exact stochastic simulations (Gillespie simulations) (86) of our model using previously used kinetic rates (see Table 1) and the following set of reactions:

$$\mathrm{G_{mRNA}} \xrightarrow{k_r} \mathrm{mRNA}$$
$$\mathrm{mRNA} \xrightarrow{g_r} \varphi$$
$$\mathrm{mRNA} \xrightarrow{k_p} \mathrm{Protein}$$
$$\mathrm{Protein} \xrightarrow{g_r} \varphi$$
$$\mathrm{Protein} + G^{OFF}_{miRNA} \underset{k_{deact}}{\overset{k_{act}}{\rightleftharpoons}} \mathrm{G^{ON}_{miRNA}}$$
$$\mathrm{G^{OFF}_{miRNA}} \xrightarrow{k_s^0} \mathrm{miRNA}$$
$$\mathrm{G^{ON}_{miRNA}} \xrightarrow{k_s} \mathrm{miRNA}$$
$$\mathrm{miRNA} \xrightarrow{g_s} \varphi$$
$$\mathrm{mRNA} - \mathrm{miRNA\ Complex} \underset{k_+}{\overset{k_-}{\rightleftharpoons}} \mathrm{mRNA} + \mathrm{miRNA}$$
$$\mathrm{mRNA} - \mathrm{miRNA\ Complex} \xrightarrow{\alpha\gamma} \varphi$$
$$\mathrm{mRNA} - \mathrm{miRNA\ Complex} \xrightarrow{\alpha(1-\gamma)} \mathrm{miRNA}.$$

where, G_{mRNA}, G^{OFF}_{miRNA}, and G^{ON}_{miRNA} denote the mRNA-coding gene, the miRNA-coding gene in off and on states, respectively. We calculated the moments of mRNA and miRNA distributions from simulations in the steady state. Below we summarize the results.

RESULTS

Feedback strength tunes the expression threshold exhibited by target mRNAs and enhances the noise around the threshold

Using the stochastic framework outlined before, we first investigated how the negative feedback affects the mean of mRNA copy numbers ($\langle r \rangle$) in the steady state. Fig. 2 *A* shows the mean mRNA obtained from the simulations as a function of the mRNA transcription rate (k_r) for different feedback strengths. Both in the absence and presence of the feedback, we found a threshold-like behavior of the mean;

TABLE 1 Description of parameters and their values

Symbol	Description	Value
k_r	mRNA synthesis rate	varied (0.0 s^{-1} - 1.0 s^{-1})
g_r	mRNA degradation rate	0.0004 s^{-1}
k_p	protein synthesis rate	0.4 s^{-1}
g_p	protein degradation rate	0.0005 s^{-1}
k_s	miRNA synthesis rate in the activated (on) state	varied (0.0 s^{-1} - 1.0 s^{-1})
k_s^0	miRNA synthesis rate in the basal (off) state	0.05 s^{-1}
g_s	miRNA degradation rate	0.0003 s^{-1}
k_+	mRNA-miRNA association rate	varied (0.001 s^{-1}-1.0 s^{-1})
k_-	mRNA-miRNA dissociation rate	0.0036 s^{-1}
γ	mRNA-miRNA complex degradation rate	0.0004 s^{-1}
α	catalyticity parameter	varied (0–1)
k_{act}	activation rate (off to on) of miRNA-coding gene	varied (0.0 s^{-1} - 0.01 s^{-1})
k_{deact}	deactivation rate (on to off) of miRNA-coding gene	0.01 s^{-1}

Parameter values are taken from (33,49). Also see the discussion on realistic parameter choice in section "materials and methods."

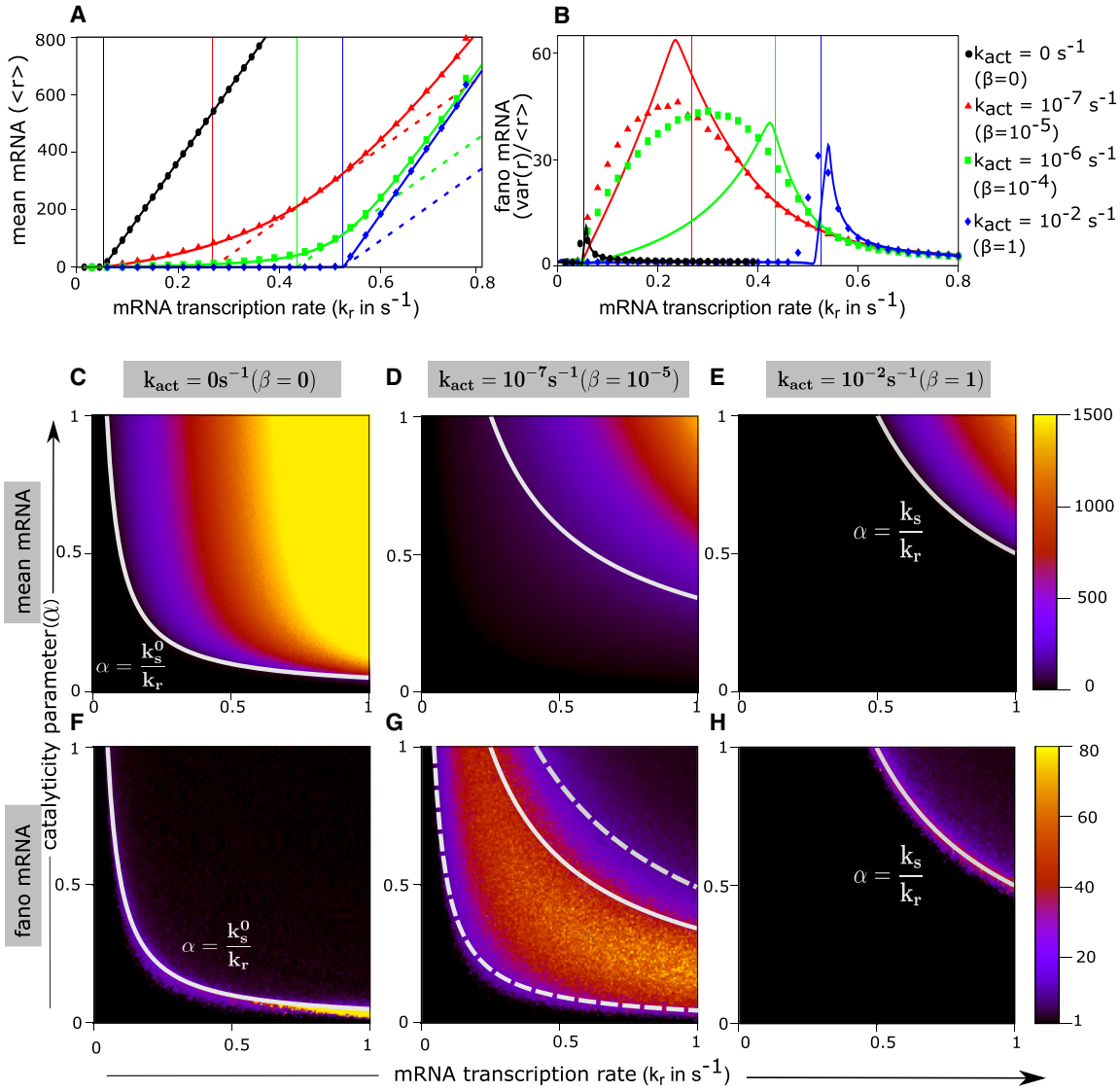

FIGURE 2 Varying negative-feedback strength modifies the expression threshold and enhances mRNA noise around the threshold. (*A* and *B*) The steady-state mean mRNA and its Fano factor are shown against mRNA transcription rate for various feedback strengths (k_{act} was varied, whereas k_{deact} was kept fixed). In (*A*) and (*B*), data points are from simulations, whereas solid curves represent solutions of the approximate moment equations (see Eq. 2 in main text; Eqs. S2.1–S2.9 and S6.1–S6.20 in Supporting material). Dashed slanted lines in (*A*) are the tangents to the mean mRNA curves (solid curves) at a point where the change in slopes are maximum; these tangents intersect the k_r axis at the threshold points. The vertical straight lines in (*A*) and (*B*) indicate respective threshold values (k_r^{th} from Eq. 3 and Eq. 5). In (*B*), the Fano factors peak near the thresholds. (*C–H*) Heat plots show mRNA means (*C–E*) and Fano factors (*F–H*) for different k_{act} in the plane of catalyticity parameter (α) and mRNA transcription rate (k_r). Color bars represent magnitudes of means and Fano factors. Analytical formula of k_r^{th} (Eq. 3 and Eq. 5) yields respective separation boundaries between low- and high-expression regimes (white curves in *C–H*). For the cases of no feedback (*F*) and high feedback (*H*), the high-noise regime coincides with the threshold boundaries. However, for low feedback strength (*G*), the high-noise regime is broadened and lies between the threshold boundaries corresponding to the limiting cases of no feedback and very high feedback (white dash curves in G re-plotted from *F* and *H*). For all panels, $k_s = 0.5s^{-1}, k_+ = 1s^{-1}$, whereas $\alpha = 0.95$ for (*A*) and (*B*). Other parameters were from Table 1. To see this figure in color, go online.

the miRNAs repress the target mRNAs making the mRNA mean almost zero up to a threshold transcription rate, and the mean increases almost linearly above the threshold. This behavior was already reported in previous studies of miRNA-based repression in the absence of feedback (33,39,49). However, when the feedback strength ($\beta = k_{act}/k_{deact}$) is varied (by changing the miRNA-gene activation rate, k_{act}), the location of the threshold changes (Fig. 2 *A*). The mean mRNA number sharply transits from low to high levels across the thresholds in the limits of no feedback and very high feedback (see the curves for $\beta = 0$ and $\beta = 1$ in Fig. 2 *A*), whereas the sharpness of transitions around thresholds decreases for intermediate feedback strengths.

To obtain the thresholds in mRNA transcription rate analytically, we derived the time-evolution equations for the mean variables from the Master equation (Eq 1) under the mean-field approximation. The mean-field equations (MFEs) are as below (see Supporting material for details):

$$\begin{aligned}
\frac{\partial\langle r\rangle}{\partial t} &\approx k_r - g_r\langle r\rangle - k_+\langle r\rangle\langle s\rangle + k_-\langle c\rangle \\
\frac{\partial\langle p\rangle}{\partial t} &\approx k_p\langle r\rangle - g_p\langle p\rangle - k_{act}\left(1 - P^{ON}\right)\langle p\rangle + k_{deact}P^{ON} \\
\frac{\partial\langle s\rangle}{\partial t} &\approx \left(k_s^0 P^{OFF} + k_s P^{ON}\right) - g_s\langle s\rangle - k_+\langle r\rangle\langle s\rangle + (k_- + (1-\alpha)\gamma)\langle c\rangle \\
\frac{\partial\langle c\rangle}{\partial t} &\approx k_+\langle r\rangle\langle s\rangle - (k_- + \gamma)\langle c\rangle \\
\frac{\partial P^{ON}}{\partial t} &\approx k_{act}P^{OFF}\langle p\rangle - k_{deact}P^{ON}
\end{aligned} \tag{2}$$

Here, the notation $\langle\cdots\rangle$ denotes the average of respective variables, and P^{ON} is the probability of the miRNA gene to be in on state. We also introduce an 'effective' mRNA-miRNA association rate defined as $g = k_+\gamma/(k_- + \gamma)$. Despite the mean-field approximation, the steady state solutions of Eq. 2 matched with the exact simulation data (see the solid curves and data points in Fig. 2 *A*).

The effect of negative feedback on the threshold behavior can be understood intuitively in the limit $g \to \infty$ (i.e., strong binding of miRNAs to mRNAs). In this limit, solving Eq. 2, we can show

$$\lim_{g\to\infty}\langle r\rangle \approx \begin{cases} 0, & \text{for } k_r < \dfrac{\left(k_s P^{ON} + k_s^0 P^{OFF}\right)}{\alpha} \\ \dfrac{\alpha\, k_r - \left(k_s P^{on} + k_s^0 P^{OFF}\right)}{\alpha\, g_r}, & \text{for } k_r \geq \dfrac{\left(k_s P^{ON} + k_s^0 P^{OFF}\right)}{\alpha} \end{cases} \tag{3}$$

where

$$P^{ON} = \frac{\beta\langle p\rangle}{(\beta\langle p\rangle + 1)} \quad \text{and} \quad P^{OFF} = \left(1 - P^{ON}\right) \tag{4}$$

From Eq. 3, the threshold mRNA transcription rate is given by $k_r^{th} = (k_s P^{ON} + k_s^0 P^{OFF})/\alpha$ (under mean-field approximation), and this mainly depends on the state probabilities of the miRNA gene (P^{ON} and P^{OFF}). The state probabilities, in turn, depend on the feedback strength ($\beta = k_{act}/k_{deact}$) and the mean protein level ($\langle p\rangle \approx (k_p/g_p)\langle r\rangle$). Thus, when the feedback strength is varied, the threshold position shifts between two extreme limits: 1) in the absence of the feedback ($\beta = 0$), the threshold is $k_r^{th} = k_s^0/\alpha$ as reported previously (33,49), and 2) in the limit of extremely high feedback ($\beta \to \infty$), the threshold becomes $k_r^{th} = k_s/\alpha$.

However, we can derive a general expression of the threshold mRNA transcription rate for any nonzero feedback strength. To this end, we first solved the MFE (Eq. 2) to obtain $\langle r\rangle$ as an explicit function of k_r, and then we defined the threshold (k_r^{th}) to be the intersection point of the k_r axis and the tangent to the mean mRNA curve drawn at a point where the change in slope is the maximum (see the dashed lines in Fig. 2 *A*, and details are in Supporting material Section S5.1). When the mRNA-miRNA effective association rate is high ($g \to \infty$), the general k_r threshold is given by

$$k_r^{th} = \frac{k_s}{\alpha} + \frac{g_r g_p}{\beta k_p} - 2g_r\sqrt{\frac{\left(k_s - k_s^0\right)}{\alpha g_r}\left(\frac{g_p}{\beta k_p}\right)} \tag{5}$$

The expression of the threshold, k_r^{th}, (Eq. 5) fairly locates the transition from low to high mean mRNA level (see the vertical lines in Fig. 2 *A* representing respective thresholds).

We next explored how the feedback strength affects the noise in mRNA copy number quantified by the mRNA Fano factor, which is the ratio of variance to the mean

($var(r)/\langle r\rangle$). As reported previously (33,49), Fano factors showed peaks around the threshold points when plotted against the mRNA transcription rate (Fig. 2 *B*). We found that negative feedback enhances the noise (i.e., peaks in Fano factors are higher) compared to the no-feedback case. Moreover, our expression of the threshold (Eq. 5) can roughly locate the positions of the peaks in Fano factors (Fig. 2 *B*). In addition to our simulation results, we numerically solved the approximate second-order moment equations (SOMEs) derived from the Master equation (Eqs. S2.1–S2.9 and S6.1–S6.20), though these solutions poorly aligned with the simulation data except for extreme cases of no feedback and very high feedback (Fig. 2 *B*, solid curves).

To understand how the catalyticity parameter (α) affects the threshold behavior, we plotted both the mean and Fano factors of mRNA copy number in the two-dimensional parameter space of $k_r - \alpha$ (see the heatmaps in Fig. 2 *C–H*). Note that our derived expression of the threshold (Eqs. 3 and 5) represents a curve in the $k_r - \alpha$ plane separating the expressed and repressed regimes in the heatmaps of mean mRNA (see solid curves in Fig. 2 *C–E*). In the Fano-factor heat maps, the high-noise regions are concentrated around the threshold curves for the limiting cases of no feedback and very high feedback (Fig. 2 *F* and *H*). For intermediate feedback strengths, the high-noise regime broadly spans around the threshold curve (see the high-intensity zone in Fig. 2 *G*). Nevertheless, the high-noise regime remains bounded within the threshold curves corresponding to the limiting cases of no feedback and very high feedback (dashed curves in Fig. 2 *G*).

Since the miRNA transcription rate in the on state (k_s) is another important parameter, we next explored how the variation of k_s modulates the expression threshold and the mRNA noise around the threshold (Fig. 2). Similarly to the derivation of a threshold mRNA transcription rate, we also derived an approximate expression of the threshold miRNA transcription rate (k_s^{th}), given by (for any nonzero feedback strength)

$$k_s^{th} = \alpha g_r\left(\frac{k_r}{g_r} - \frac{g_p}{\beta k_p}\right) + 2\alpha g_r\sqrt{\frac{g_p\left(\alpha k_r - k_s^0\right)}{\alpha\beta g_r k_p}} \quad (6)$$

For very high feedback ($\beta \to \infty$), the expression of k_s^{th} simplifies to $k_s^{th} = \alpha k_r$ (however, k_s has no role for the no-feedback case as the miRNA production happens always at the basal rate, k_s^0). The expression of k_s^{th} again correctly identified the separation between the expressed and repressed regimes in the $k_s - \alpha$ plane (see heat plots of the mean mRNA in Fig. 3 *A–C*). Also, the high-noise regimes spanned around the curves of k_s^{th} in heat plots of Fano factors (Fig. 3 *D–F*). As before, for intermediate feedback strengths, the high-noise regime is broader than the limiting cases, and it is bounded within the corresponding threshold curves of the limiting cases (see dashed curves in Fig. 3 *E*).

We further investigated the role of the association between mRNAs and miRNAs in the transitions of expression levels around the thresholds (Figs. S1 and S2). We found that a higher effective association rate (g) mainly led to a more sharpened transition (see Fig. S1 *A*). Moreover, lowering the effective association rate decreases the overall mRNA noise (see Figs. S1 *F–H* and S2 *D–F*).

Together, we conclude that tuning the negative-feedback strength modifies the threshold locations separating the high and low mean expressions. On the other hand, the effective association of miRNAs with the mRNAs largely determines the sharpness of the transition at the thresholds. Moreover, the mRNA noise peaks near the thresholds, suggesting that the mRNA distributions could pass through qualitatively distinct regimes across the threshold points.

Bimodal mRNA distributions around the threshold

We next asked how the mRNA distribution changes across the expression threshold in the steady-state when the miRNA transcription rate is varied. We first focused on a regime where the miRNA-mRNA association is strong (i.e., $k_+ \gg (k_- + \gamma)$, implying a high g) and the feedback strength is high (i.e., high $\beta = k_{act}/k_{deact}$). In this regime, the steady state means of mRNA and miRNA showed sharp transitions around the threshold ($k_s^{th} \sim \alpha k_r$), and they exhibited opposing trends with increasing miRNA transcription rate (k_s); see Fig. 4 *A*. The mean mRNA ($\langle r\rangle$) is higher than the mean miRNA ($\langle s\rangle$) below k_s^{th}, whereas $\langle s\rangle$ is higher than $\langle r\rangle$ above k_s^{th} ($k_s^{th} \sim 0.655 s^{-1}$). The miRNAs and mRNAs are equal to each other on average at the threshold (Fig. 4 *A*), where both are present in small copy numbers, suggesting that their coupled number fluctuations become vital near the threshold. Correspondingly, the correlation between mRNAs and miRNAs (quantified by the Pearson correlation coefficient, $\rho = (\langle rs\rangle - \langle r\rangle\langle s\rangle)/\sigma_r\sigma_s$, where σ_r and σ_s are standard deviations) showed a sharp deep at the threshold point (Fig. 4 *B*), signifying high anti-correlation between mRNAs and miRNAs. Thus, due to strongly coupled and enhanced number fluctuation near the threshold, mRNAs randomly switch between 'miRNA-bound' and 'miRNA-unbound' states biasing either repression or expression respectively, which in turn could generate substantial expression variability. Accordingly, the steady-state mRNA distribution became bimodal near the threshold (Fig. 4 *C*); however, the distribution was bell-shaped (approaching a Poisson-like shape) above the threshold, and it was like an exponential below the threshold (in the repressed regime). This shape transition of mRNA distributions could be further elucidated by simulating the time traces of the free miRNA and mRNA molecules across the threshold (see Fig. 4 *D–F*). As anticipated, both miRNAs

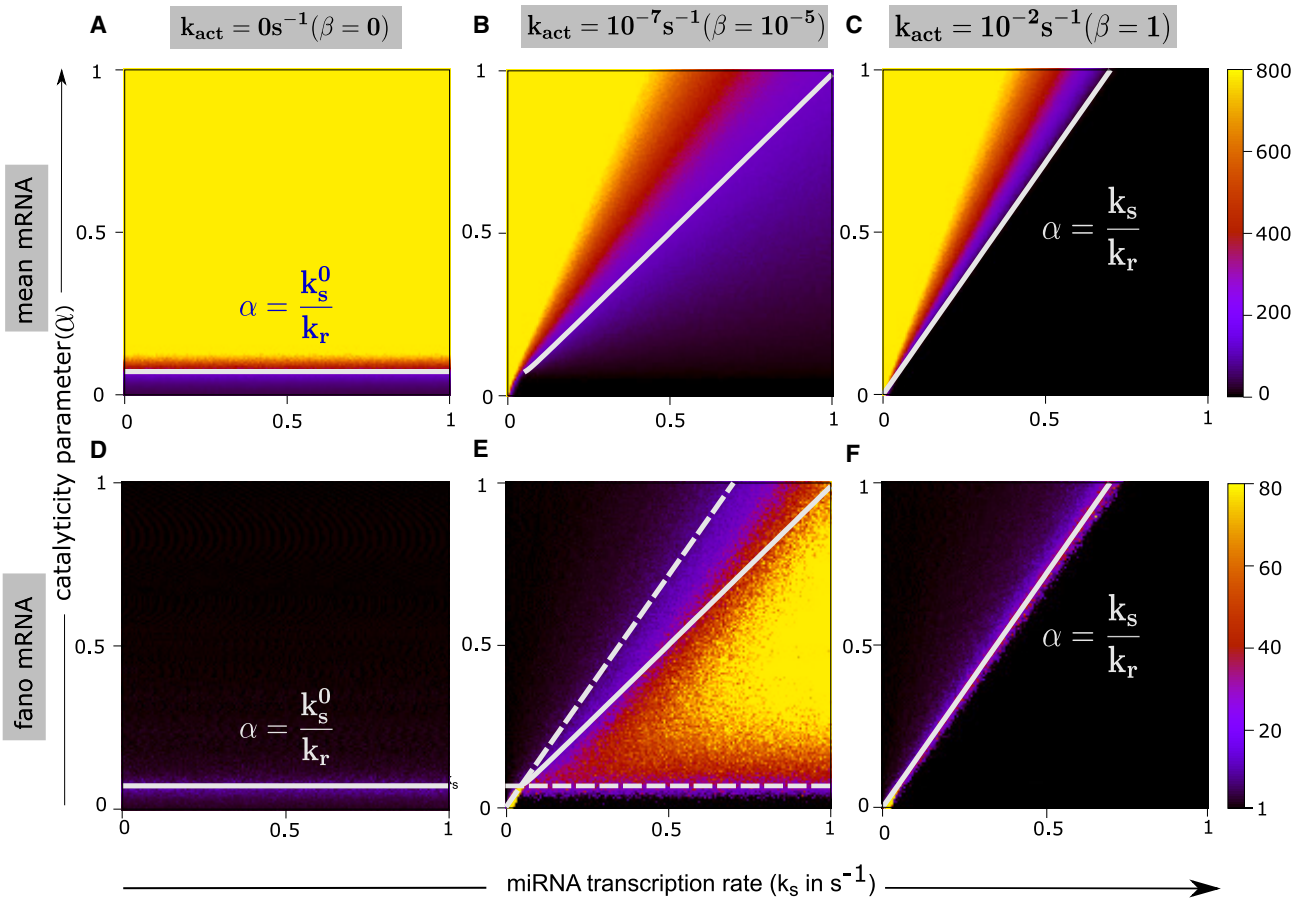

FIGURE 3 Effects of varying miRNA transcription rate on expression thresholds and Fano factors for different feedback strengths. Heat plots of steady-state means (*A–C*) and Fano factors (*D–F*) are shown in the $k_s - \alpha$ plane for different k_{act}. Similar to Fig. 2, we observed expression thresholds and high noise around these thresholds. The solid white line in each plot locates the threshold curves (k_s^{th} from Eq. 6). In (*E*), the high-noise regime lies between two limiting threshold boundaries corresponding to no-feedback and high-feedback cases (white dashed lines in *E* are re-plotted from *D* and *F*). Parameters are $k_r = 0.7 s^{-1}, k_+ = 1 s^{-1}$, and others were taken from Table 1. To see this figure in color, go online.

and mRNAs showed high anticorrelated fluctuations near the threshold, toggling stochastically between almost zero and nonzero numbers (see Fig. 4 *E*). However, only one species (either mRNA or miRNA) dominated the other away from the threshold (Fig. 4 *D* and *F*).

Since the miRNA-coding gene switches between on (activated) and off (basal) states due to negative feedback, we also checked how the miRNA gene states behave across the threshold where bimodal expression was observed. Note that free mRNAs dominate over the miRNAs below the threshold (Fig. 4 *A*), and hence the proteins translated from free mRNAs could push the miRNA gene mostly into the on state. This expectation was consistent with the observed behavior of state probabilities (P^{ON} and P^{OFF}) across the threshold (Fig. 4 *B*). We further monitored the time traces of miRNA gene states (denoted by 1 for on and 0 for off), shown in Fig. 4 *G–I*. Below the threshold, the miRNA gene was in on state (Fig. 4 *G*), and it mostly was in off state above the threshold (Fig. 4 *I*). The time traces of miRNA gene states further raise the question: how does the protein-dependent state switching of the miRNA gene modulate the "bursty" behavior of miRNA synthesis across the threshold?

Bursty nature of miRNA synthesis across the threshold

It is well known that the waiting time distribution for individual transcription events markedly deviates from a simple exponential when the RNA synthesis is bursty, giving rise to multiple timescales (12,87). Following Dobrzynski et al. (87), we calculated the distribution of waiting times (i.e., intervals between consecutive miRNA production events). Interestingly, when the miRNA synthesis rate goes above the threshold (k_s^{th}), the waiting time distribution is biphasic (described by a sum of two exponentials), but it becomes a simple exponential below the threshold (see Fig. 4 *J*). This behavior stems from the fact that the miRNA gene is mainly in the activated (on) state below the threshold (silencing the target mRNAs) but often switches between off and on states above the threshold (Fig. 4 *G–I*).

We also derived an approximate expression for the waiting time distribution by considering a two-state miRNA gene without protein-dependent activation (see in Supporting material), given by

$$q(t) \approx \omega_1 k_1 e^{-k_1 t} + \omega_2 k_2 e^{-k_2 t} \tag{7}$$

where $k_{1,2} = \frac{1}{2}[(k_{deact} + \langle p \rangle k_{act} + k_s^0 + k_s) \pm \delta]$ and

$$\omega_1 = \frac{1}{k_1}\left[\frac{k_s \langle p \rangle k_{act}}{2\lambda\delta}\left\{k_{deact}\left(k_s - 2k_s^0\right) + k_s\left(\delta - \langle p \rangle k_{act} - k_s^0 + k_s\right)\right\} + \frac{k_s^0 k_{deact}}{2\lambda\delta}\left\{k_s^0\left(\delta - k_{deact} + \langle p \rangle k_{act} + k_s^0\right) - k_s\left(2\langle p \rangle k_{act} + k_s^0\right)\right\}\right],$$

$$\omega_2 = \frac{1}{k_2}\left[\frac{k_s \langle p \rangle k_{act}}{2\lambda\delta}\left\{-k_{deact}\left(k_s - 2k_s^0\right) + k_s\left(\delta + \langle p \rangle k_{act} + k_s^0 - k_s\right)\right\} + \frac{k_s^0 k_{deact}}{2\lambda\delta}\left\{k_s^0\left(\delta + k_{deact} - \langle p \rangle k_{act} - k_s^0\right) + k_s\left(2\langle p \rangle k_{act} + k_s^0\right)\right\}\right],$$

with

$$\lambda = \left(k_s \langle p \rangle k_{act} + k_s^0 k_{deact}\right),$$

$$\delta = \sqrt{\left(k_{deact} + \langle p \rangle k_{act} + k_s^0 + k_s\right)^2 - 4\left(k_s \langle p \rangle k_{act} + k_{deact} k_s^0 + k_s^0 k_s\right)}$$

Here, $\langle p \rangle$ is the mean protein number, which is calculated from the solution of the approximate SOMEs (Eqs. S2.1–S2.9 and S6.1–S6.20 in Supporting material). Note that Eq. 7 is a weighted sum of two exponentials, signifying two timescales above the threshold: a short timescale representing the interval between successive miRNA synthesis during rapid synthetic activity and a longer timescale of synthetic inactivity. Thus, we can define a point of timescale separation as $\tau_s = \frac{1}{(k_1 - k_2)} ln\left(\frac{\omega_1}{\omega_2} \cdot \frac{k_1}{k_2}\right)$, where two terms in Eq. 7 become equal. Due to the timescale separation, we can define the burst size as (87,88)

$$b = \frac{\text{number of total miRNA synthesis events}}{\text{number of intervals longer than} \tau_s}$$

Using this definition, we can express b from Eq. 7 as below

$$b = \left[\omega_1 \left(\frac{\omega_2}{\omega_1} \cdot \frac{k_2}{k_1}\right)^{\frac{k_1}{k_1 - k_2}} + \omega_2 \left(\frac{\omega_2}{\omega_1} \cdot \frac{k_2}{k_1}\right)^{\frac{k_2}{k_1 - k_2}}\right]^{-1} \tag{8}$$

Moreover, following (87), we define the burst duration as

$$\tau_b = b\langle T_{\leq \tau_s} \rangle, \tag{9}$$

where $\langle T_{\leq \tau_s} \rangle$ denotes the average intervals shorter than τ_s, yielding the average waiting time of miRNA production within a burst (or, equivalently, the mean of the fast timescale).

As shown in Fig. 4 *K–L*, we calculated the burst size and burst duration from simulations and compared them with our approximate expressions (Eqs. 8 and 9, along with Eq. S9.4–S9.6; see Section 9 in Supporting material), which matched reasonably well. Note that burst size and duration are undefined below k_s^{th} as there is no timescale separation; hence, these quantities diverge near the threshold (Fig. 4 *K–L*), indicating an alternative way of locating the threshold point. We further derived simple asymptotic expressions of burst size and duration for high values of miRNA synthesis rate (k_s). At $k_s \to \infty$, these quantities become

$$b \approx \frac{\langle p \rangle k_{act} k_s}{k_{deact}\left(k_s^0 + \langle p \rangle k_{act}\right)} \tag{10}$$

$$\tau_b \approx \frac{\langle p \rangle k_{act}}{k_{deact}\left(k_s^0 + \langle p \rangle k_{act}\right)}, \tag{11}$$

which also matched well with simulation data (Fig. 4 *K–L*).

Intuitively, the miRNA gene is expected to be in the off state when the feedback is negligible, whereas it could be mostly in the on state for very high feedback (see Eq. 4). Between these two extreme limits, the state switching of the miRNA gene could be much more frequent, leading to expression variability. Therefore, two different processes could collectively modulate the emergence of bimodality: 1) the switching between miRNA-bound and miRNA-unbound states of free mRNAs near the threshold, i.e., the

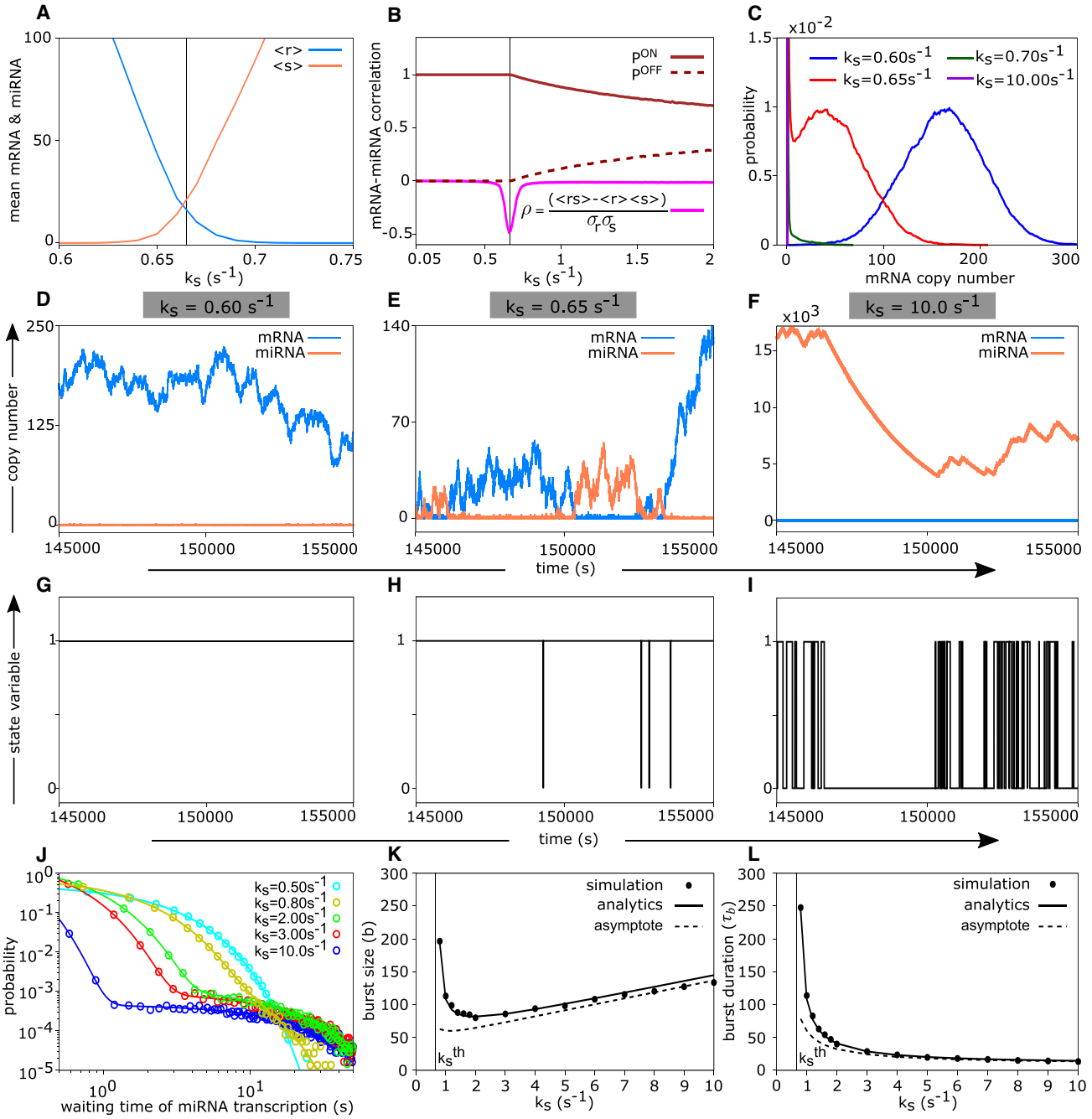

FIGURE 4 Bimodal mRNA distribution and bursty miRNA synthesis near the threshold. (*A*) Transitions of mean mRNA and mean miRNA are shown against miRNA transcription rate (k_s). (*B*) The mRNA-miRNA Pearson correlation (ρ) versus k_s. The probabilities of the miRNA gene to be in the activated state (P^{ON}) or basal state (P^{OFF}) are also shown. The black vertical lines in (*A*) and (*B*) indicate the threshold (k_s^{th}), where mRNA-miRNA correlation showed a sharp deep in (*B*). (*C*) Steady-state mRNA distributions spanning the threshold region. Note the bimodal distribution near the threshold (red curve). (*D–F*) Temporal evolution of mRNA copy number ($r(t)$) and miRNA copy number ($s(t)$) at different k_s values across the threshold. Around the threshold, miRNAs and mRNAs are present in small numbers and show large anticorrelated fluctuations (*E*). Away from the threshold, either mRNA or miRNA dominates over the other (*D* and *F*). (*G–I*) Time traces of the miRNA-gene state at different k_s values spanning the threshold, k_s^{th}. Here, 1 and 0 denote activated (on) and basal (off) states, respectively. In (*D*)–(*I*), the same time windows were chosen to make correspondence. (*J*) Log-log plots of waiting time distributions for miRNA synthesis across the threshold, showing biphasic nature above the threshold ($k_s^{th} \sim 0.66 s^{-1}$ here). (*K* and *L*) Burst size (*K*) and burst duration (*L*) are plotted against k_s. Data points are from simulations, solid curves are from approximate analytical formulas (Eqs. 8 and 9 in the text), and dashed curves represent asymptotic expressions (Eqs. 10 and 11). Vertical lines denote the threshold locations. We used high feedback and high miRNA-mRNA association strength ($k_{act}/k_{deact} = 1$ and $k_+/k_- \approx 278$), whereas other parameters were from Table 1. To see this figure in color, go online.

complex formation and dissociation dynamics (governed by the effective association rate, g), and 2) the switching between on (activated) and off (basal) states of the miRNA gene (governed by the feedback strength, β).

Tuning miRNA-mRNA association and feedback strength modulate the emergence of bimodality

We asked how the effective association rate ($g = k_+\gamma/(k_- + \gamma)$) and the feedback strength ($\beta = k_{act}/k_{deact}$) affect the emergence of bimodal mRNA distributions in the steady state. To this aim, we systematically varied the mRNA-miRNA binding/unbinding rate (k_+ or k_-) and the miRNA gene activation rate (k_{act}) to monitor how the mRNA distributions change across the expression threshold. Specifically, for a wide range of g ($0.0001s^{-1} - 0.1s^{-1}$) and β (0 − 1), we first identified the threshold mRNA transcription rate (k_r^{th}) and then investigated the mRNA distributions across the threshold (see Fig. 5). For a strong miRNA-mRNA association ($g \sim 0.01s^{-1} - 0.1s^{-1}$), bimodal mRNA distributions appeared near the threshold irrespective of the absence and presence of feedback (i.e., for both $\beta = 0$ and $\beta \neq 0$) (see Fig. 5 *A–F*). Thus, for a strong miRNA-mRNA association, the switching between miRNA-bound and unbound states of the mRNAs primarily leads to bimodal distributions since bimodality was already present in the no-feedback case (Fig. 5 *A* and *D*), and bimodality persisted when feedback was introduced. On the other hand, for a minimal miRNA-mRNA association ($g = 0.0001s^{-1}$), bimodality disappeared both in the presence and absence of feedback (see Fig. 5 *M–O*) as miRNAs hardly bound with mRNAs in this regime. More interestingly, for intermediate level of miRNA-mRNA association ($g \sim 0.0004s^{-1} - .001s^{-1}$), bimodal distributions emerged only when the feedback strength was intermediate (see Fig. 5 *H* and *K*), whereas bimodality disappeared for the extreme cases of no feedback (Fig. 5 *G* and *J*) and very high feedback (Fig. 5 *I* and *L*). These observations suggest that the switching between on (activated) and off (basal) states of the miRNA gene could be the determining factor for the bimodality when the miRNA-mRNA association (g) was intermediate. Note that the miRNA gene was always in the off (basal) state in the no-feedback case. However, for an intermediate feedback strength, the miRNA gene's average residency time in the off and on states kept changing across the threshold (see Fig. 6 *A–F*, corresponding to Fig. 5 *H*). Below the threshold ($k_r < k_r^{th}$), the mean mRNA (and correspondingly translated TFs) was low, and hence the miRNA gene mainly was in the off state (Fig. 6 *A* and *D*). Conversely, the miRNA gene was largely in the on state above the threshold as the mean mRNA and translated TFs were high (Fig. 6 *C* and *F*). Near the threshold, the miRNA gene spent almost the same amount of time in on and off states, leading to the mRNA copy number variability and subsequent bimodality. In contrast, such frequent toggling between on and off states could not occur when the feedback strength was very high; here, the miRNA gene mostly stayed in the on state across the threshold (see Fig. 6 *G–L*, corresponding to Fig. 5 *I*), reducing the heterogeneity in expression. Therefore, the miRNA-gene state switching (due to negative feedback) plays a key role in modulating bimodality for an intermediate miRNA-mRNA association rate.

We thus conclude that 1) negative-feedback strength (β, controlling the miRNA gene state switching) and 2) the effective association rate (g, controlling the mRNA-miRNA binding strength) are the main governing factors for bimodal distributions. Following Jia et al. (89), we further quantified the strength of bimodality by a parameter κ ($0 < \kappa < 1$), defined as

$$\kappa = \left(H_{low} - H_{valley}\right) / H_{high}. \quad (12)$$

Here, H_{low}, H_{high}, and H_{valley} denote the lower peak height, the higher peak height, and the height of the valley between them, respectively. We represented the κ values as a heat map in the $k_r - k_+$ parameter space (see Fig. 6 *M–O*). In the intermediate feedback strength, the parameter regime of observing bimodality gets broadened (Fig. 6 *N*) compared to no-feedback and high-feedback cases. Thus, for intermediate feedback, prominent bimodality could also be observed for low miRNA-mRNA association strength, not only for a strong miRNA-mRNA association (Fig. 5 *H*, *K*, and 6 *M*).

A question naturally arises as to how the miRNA-mediated repression compares with a simple auto-repression (i.e., a gene producing its own repressors) since both motifs are ubiquitous in various biological contexts.

A comparison of miRNA-mediated negative feedback with an auto-repression

There already exist several theoretical (77,81,82,90–92) and experimental studies (79,80) of auto-regulatory negative feedback where a gene expresses its repressor. A general understanding is that an auto-regulatory negative-feedback motif can buffer the gene expression noise (79–82), but an auto-regulatory positive-feedback motif generally exhibits bistability in expression (71,75,76,78,93–95).

Here, we revisited a model of an auto-repression motif to compare it with our model of miRNA-mediated negative feedback (see Fig. 7 *A* and *B*). Note that the motif of miRNA-mediated negative feedback represents a scenario of indirect repression (i.e., repression through intermediate steps of miRNA-gene activation; Fig. 7 *A*). In contrast, the simple negative feedback represents direct repression or auto-repression, where the gene produces a protein (repressor) that binds with the same gene and reduces its transcription rate from the basal rate (Fig. 7 *B*). In this auto-repression motif, the binding and unbinding rates of the repressor are k_{off} and k_{on}, respectively. The repressor-bound

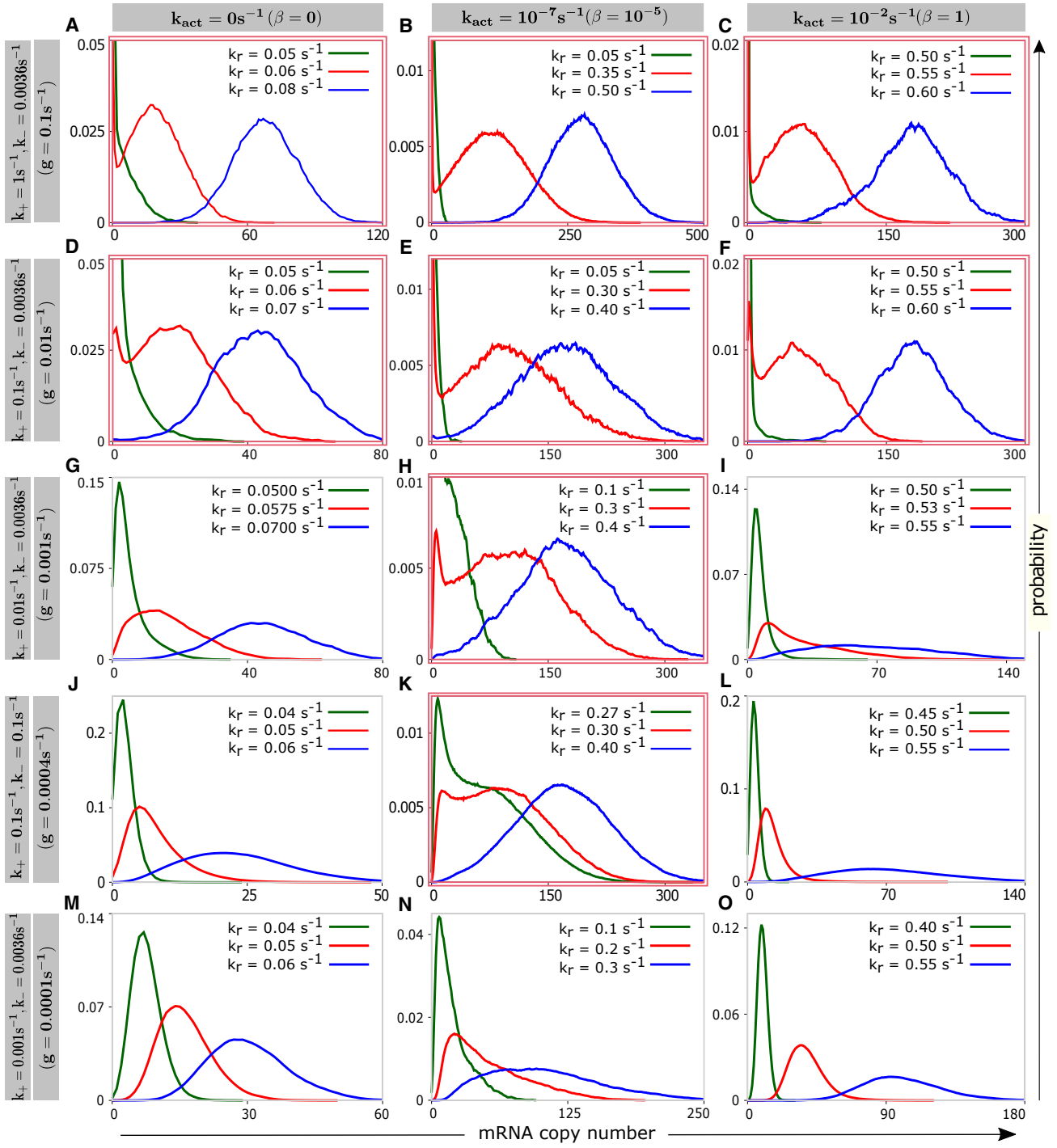

FIGURE 5 Effects of miRNA-mRNA binding affinity and feedback strength on the emergence of bimodality. Steady-state mRNA distributions at different mRNA transcription rates (k_r) are shown by varying the miRNA-mRNA association/dissociation rate (k_+ or k_-) and the activation rate of the miRNA-coding gene (k_{act}). For strong miRNA-mRNA association, bimodal mRNA distributions appeared both in the absence and presence of feedback (*A–F*). Conversely, bimodality disappeared for a weak miRNA-mRNA association (*M–O*). For intermediate association strength, bimodal distributions did not emerge for the limiting cases of no feedback (*G* and *J*) and very high feedback (*I* and *L*); bimodality emerged only when the feedback strength was intermediate (*H* and *K*). We used $k_- = 0.1 s^{-1}$ for (*J*)–(*L*) and for the rest of the panels $k_- = 0.0036 s^{-1}$. k_+ and k_{act} are varied as shown. $\alpha = 0.95$ and other parameters were from Table 1. Panels containing bimodal distributions are marked with red double-lined border. To see this figure in color, go online.

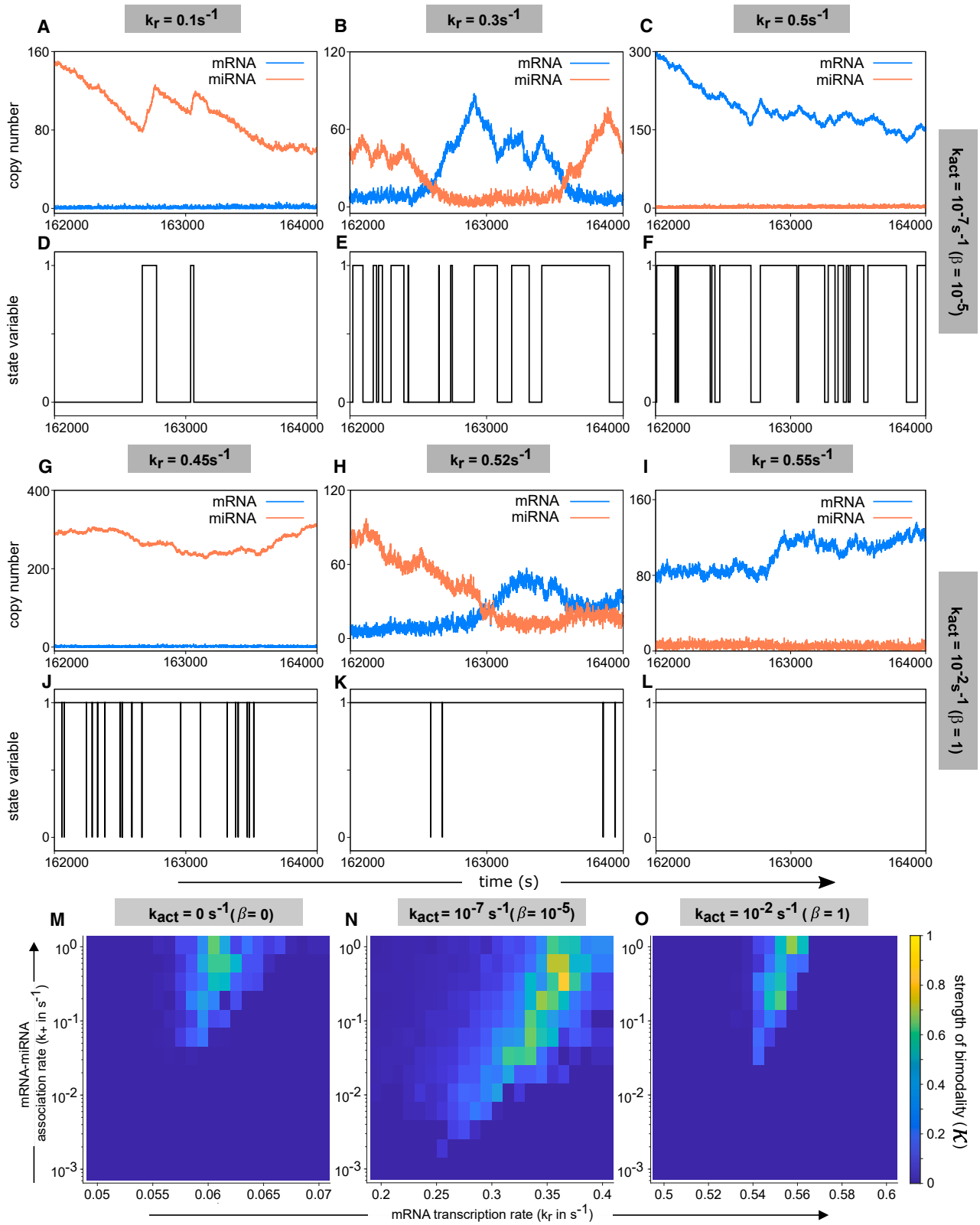

FIGURE 6 State switching of the miRNA gene and stochastic time traces can explain the unimodal-bimodal phase diagram. Switching of the miRNA gene and time traces of miRNAs and mRNAs are shown for an intermediate level of miRNA-mRNA effective association ($g = 0.001s^{-1}$). (*A*)–(*F*) are for $\beta = 10^{-5}$ corresponding to Fig. 5 *H*; whereas (*G*)–(*L*) correspond to Fig. 5 *I* for a very high feedback strength ($\beta = 1$). For $\beta = 10^{-5}$, we observed anti-correlated fluctuations in mRNA and miRNA numbers near the threshold (*B*) and frequent toggling of the miRNA gene between on and off states (*E*),

(legend continued on next page)

gene transcribes mRNAs at a lower rate (k_r^{low}), and the transcription rate for the repressor-unbound gene is higher (k_r^{high}).

To compare the outputs of the two motifs on an equal footing, we first set the same protein synthesis rate and the same degradation rates of mRNAs and proteins in both motifs (k_p, g_p, and g_r in Fig. 7 *A* and *B*). We then chose other parameters in such a way that, in both motifs, the mean mRNA levels are the same in the limit of no feedback (when $k_{act}/k_{deact} \to 0$ or $k_{off}/k_{on} \to 0$ in respective motifs; see Fig. 7 *A* and *B*). These limiting means are roughly $\langle r \rangle \approx (k_r/g_r - k_s^0/\alpha g_r)$ for the miRNA-mediated repression (Eq. 3) and $\langle r \rangle \approx k_r^{high}/g_r$ for the auto-repression. We further noted that increasing k_{off} (i.e., the deactivation rate of the target gene by repressors) biases the auto-repression motif toward a low expression regime (Fig. 7 *B*), whereas increasing k_{act} (i.e., the activation rate of the miRNA gene by proteins) pushes the miRNA-mediated repression motif toward low expression. Thus, increasing k_{off} or k_{act} in respective motifs can increase the negative-feedback strengths (when other parameters are fixed). We, therefore, varied k_{off} or k_{act} in respective motifs and calculated the steady state mean mRNA and its Fano factors, as shown in Fig. 7 *C* and *D*. As expected, both motifs exhibited similar transitions of mean mRNAs from high to low values when the bias toward repression was increased by varying respective feedback strengths (Fig. 7 *C* and *D*). The Fano factors also peaked near the cross-over region (see insets, Fig. 7 *C* and *D*). Thus, both motifs are qualitatively indistinguishable at the mRNA mean and noise level. However, when we monitored the steady-state mRNA distributions across the peak regions of Fano factors, the bimodal distribution was observed in the miRNA-mediated repression (Fig. 7 *E*), but the auto-repression did not produce bimodality (Fig. 7 *F*). In fact, it was known from a recent experiment (80) that direct negative feedback or auto-repression does not produce bimodal distributions. On the contrary, as discussed in the previous section, the bimodality in miRNA-mediated repression stems from the frequent switching of miRNA gene between on (activated) and off (basal) states near the high Fano-factor region, whereas one of the states dominated away from this region (Fig. S3). Together, we conclude that the indirect negative feedback via miRNAs can potentially generate phenotypic diversity compared to direct negative feedback.

DISCUSSION

Summary

Negative-feedback loops involving miRNAs are often found in several gene regulatory networks governing diverse cellular processes such as cell differentiation and cancer progression (34–38,58–61,63,65). To investigate the effects of a miRNA-mediated SNFL, we here built a stochastic framework describing the competitive titration between miRNAs and their target mRNAs. Earlier theoretical studies have suggested that there are essentially three factors governing gene expression in miRNA-dependent SNFL (68−70): 1) activation and deactivation of the miRNA-coding gene by the TF, 2) association-dissociation between miRNAs and target mRNAs, and 3) miRNA's catalytic mode of action on target mRNAs. However, previous models did not incorporate the above three factors altogether. In contrast, our detailed model incorporates all these factors (Fig. 1). In our model, a gene produces a specific protein that acts as a transcriptional activator of a miRNA-coding gene and, in turn, the miRNA suppresses the TF itself. The output of the motif largely depends on three key parameters: the negative-feedback strength (denoted by $\beta = k_{act}/k_{deact}$), the effective miRNA-mRNA association rate ($g = k_+\gamma/(k_- + \gamma)$), and the catalyticity parameter (α). A systematic analysis by varying these parameters revealed some interesting aspects of miRNA-mediated negative feedback.

With increasing mRNA transcription rate (or decreasing miRNA transcription rate), the mean mRNA at the steady state showed a threshold-like behavior transiting from a low to a high level (Figs. 2 *A*, *C–E*, and 3 *A–C*). Such behavior was previously observed in experiments, and theoretical studies that did not incorporate feedback (33,39,49). The presence of negative feedback further modifies the threshold points, which we found analytically using mean-field approximation (Eqs. 5 and 6). We also quantified the gene expression noise at the steady state by the mRNA Fano factor ($var(r)/\langle r \rangle$). This intrinsic noise displayed a peak in the vicinity of the threshold (Fig. 2 *B*) similar to the previous study in the absence of feedback (49). However, feedback enhances the noise near the respective thresholds (Fig. 2 *B*).

Away from the threshold, one species (either miRNA or mRNA) dominates another, but, in the proximity of the threshold, their copy numbers are low and near equal (Fig. 4 *A*), representing a titration-like binding process to form miRNA-mRNA complexes. The miRNA-mRNA titration introduces a negative correlation between these two species that is enhanced at the expression threshold (Fig. 4 *B*). Either all of the miRNAs or mRNAs are fully bound in miRNA-mRNA complexes away from the threshold. Near the threshold, however, mRNAs stochastically become free or miRNA bound, leading to large anticorrelated fluctuations of miRNA and mRNA numbers (Fig. 4 *D–F*). This stochastic fluctuation between expressed and repressed

corresponding to the bimodal mRNA distribution (in Fig. 5 *H*). Increasing the feedback strength creates a bias toward the on state (*J–L*). For a high feedback strength, the frequency of state toggling near the threshold is markedly reduced (compare *E* and *K*). (*M–O*) Heatmaps showing bimodality strength, κ (calculated from Eq. 12), in the $k_r - k_+$ plane for different feedback strengths. Parameters: $k_s = 0.5s^{-1}, k_+ = 0.01s^{-1}$ for A − L, $\alpha = 0.95$. Other parameters from Table 1. To see this figure in color, go online.

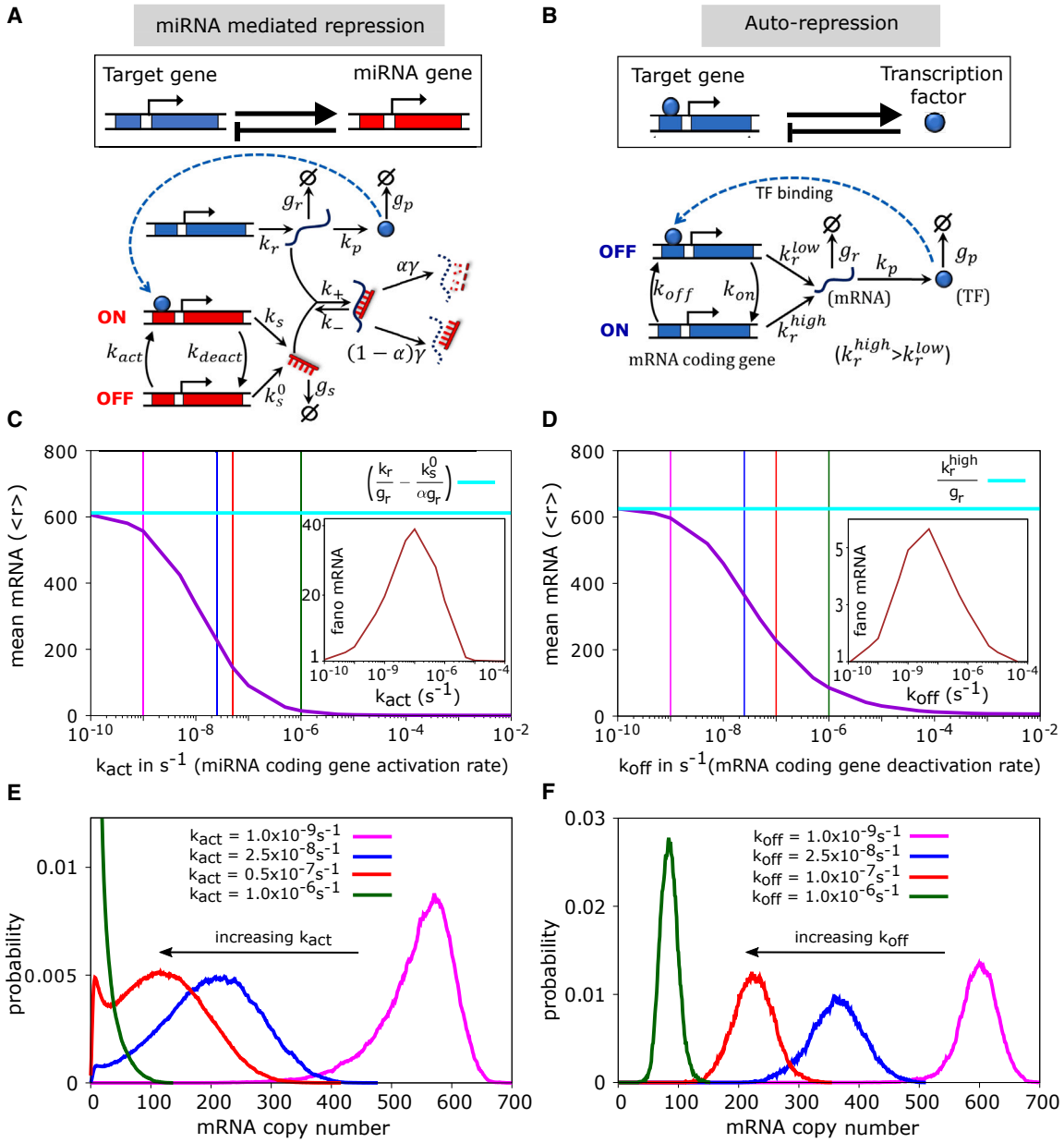

FIGURE 7 A comparison of miRNA-mediated negative feedback with auto-repression shows distinctive features in target mRNA distributions. (*A*) Our model of a miRNA-mediated negative-feedback loop (same as in Fig. 1). (*B*) Schematic and detailed model of a negative auto-regulatory motif where a gene produces its own repressor. In (*A*), the miRNA production increases as k_{act} increases, which in turn suppresses target mRNAs. In (*B*), for higher k_{off}, the mRNA production rate switches from k_r^{high} to k_r^{low}. Thus, both k_{act} and k_{off} produce a bias toward repression in respective motifs, when k_{deact} and k_{on} are fixed. (*C* and *D*) Steady state Means and Fano factors of mRNA are shown by varying k_{act} (for miRNA-mediated negative feedback) and k_{off} (for auto-repression). In both cases, means cross over from high- to low-expression regimes as the bias toward repression increases, and the Fano factors peak near the crossover region. The vertical lines in (*C*) and (*D*) represent the locations where mRNA distributions were sampled and are shown in (*E*) and (*F*). (*E* and *F*) Steady-state mRNA distributions for respective motifs. Parameter values of k_p, g_p, and g_r were the same in both motifs (as in Table 1), whereas other parameters were chosen in such a way that the mean curves look similar in both cases. Parameters for (*C*) and (*E*) were $k_r = 0.25s^{-1}$, $k_s = 0.5s^{-1}$, $k_s^0 = 0.005s^{-1}$, $k_+ = k_- = 0.1s^{-1}$, and $\alpha = 0.95$, whereas others were from Table 1. For (*D*) and (*F*), we used $k_r^{high} = 0.25s^{-1}$, $k_r^{low} = 0.0025s^{-1}$, $k_{on} = 0.01s^{-1}$. To see this figure in color, go online.

states (Fig. 4 *E*) is manifested as a noise-induced bimodality in mRNA distributions (Fig. 4 *C*) in the proximity of the threshold. This emergence of bimodality can be further tuned by the strength of negative feedback and the miRNA-mRNA association rate (Figs. 5 and 6 *M*).

Next, we quantitatively compared our model with an auto-repression (Fig. 7 *A* and *B*). In miRNA-mediated negative feedback, the suppression of transcription factors occurs indirectly via miRNAs, whereas, in auto-repression, TFs directly suppress themselves, acting as repressors of their gene. In

both circuits, as expected, the mean mRNA displayed a transition from high to low expression with increasing negative-feedback strength, and the mRNA Fano factor increased around the transition region (Fig. 7 *C* and *D*). Comparing the peak heights of the mRNA Fano factor, we could conclude that miRNA-mediated feedback is noisier than auto-repression; this is in line with previous results that auto-repression suppresses heterogeneity of gene expression (79–82). Although the target gene expression exhibited similar characteristics at the mean and noise level, the contrast between these two types of negative-feedback circuits lies at the distribution level (Fig. 7 *E* and *F*). The miRNA-mediated negative feedback produced bimodality in mRNA distributions, whereas auto-repression did not, suggesting the crucial roles of miRNAs in generating phenotypic diversity.

Biophysical relevance

The miRNA-mediated negative-feedback loop for TFs has been reported in various biological contexts. For instance, in midbrain dopaminergic neuron maturation, the TF PITX3 activates miR-133, which inhibits PITX3 (65). Similar feedback loops have been reported in cell cycle regulation between the TF E2F and its targets (96). Such feedback loops can prevent abnormal accumulation of TFs, thus fine-tuning dynamic cellular responses. In this scenario, the bimodality of gene expression can allow multiple metastable cell states to coexist with two different expression values associated with distinct phenotypes.

We showed that two distinct processes control the bimodality of mRNA distributions in a miRNA-based negative-feedback loop: 1) switching of target mRNAs between miRNA-bound and miRNA-free states (captured by the effective miRNA-target association rate, g), and 2) the TF-dependent switching of miRNA-coding gene between basal (off) and activated (on) states (quantified by the feedback strength β). Thus, two parameters (g and β) collectively modulate the emergence of bimodal mRNA distributions (Fig. 5). We also quantified the bimodality strength (κ) in a 2D phase diagram (Fig. 6 *M–O*), linking model parameters with quantitative prediction. We further investigated if the bimodality observed at the mRNA level would also be translated at the protein level. We found that the steady-state protein distributions became prominently bimodal with increasing protein degradation rate at a fixed protein synthesis rate (Fig. S4).

We checked how bimodality changes by systematically increasing the switching rates of miRNA gene states (k_{act} and k_{decat}). We numerically investigated the limits $k_{act} \to \infty$ and $k_{deact} \to \infty$ by keeping the feedback strength constant at an intermediate level ($\beta = k_{act}/k_{decat} = 10^{-5}$). The bimodality persisted for high miRNA-mRNA association strength even when k_{act} and k_{decat} were large (see Fig. S5 *A–C*). In contrast, for low miRNA-mRNA association strength, the bimodality is visible only when k_{act} and k_{decat} are small, and bimodality vanishes for very large k_{act} and k_{decat} (Fig. S5 *D–F*). Since, irrespective of the state of the miRNA-coding gene, the switching of target mRNAs between 'miRNA-bound' and 'miRNA-unbound' states modulates the proportion of blocked and free mRNAs; bimodality can always be observed if the miRNA-mRNA effective association rate (g) is high enough (as in Fig. S5 *A–C*). On the other hand, when miRNA-mRNA association is weaker, the feedback strength (β) mainly modulates the target-protein-dependent switching of the miRNA-coding gene between off and on states. Hence, bimodality can only be observed in the medium feedback, where the state switching dominates near the threshold (rather than remaining mostly in the basal or activated states). In this case, when the state-switching rates are very large compared to other parameters, the miRNA gene cannot stay in one particular state (either basal or activated) for a sufficiently long time, and hence the system cannot sample the relative abundances of target mRNAs regulated by the distinct synthetic activity of the miRNA gene. The above understanding provides an insightful distinction between our model and a simple auto-regulation.

In contrast to our findings, another theoretical study on miRNA-based negative feedback reported bell-shaped or long-tailed unimodal distributions of proteins (70). This difference may arise due to the coarse-grained modeling in the latter study as compared to our detailed modeling. On the other hand, deterministic modeling of miRNA-based negative feedback (69) missed the rich interplay between negative feedback and miRNA-target titration in modulating gene expression noise, as elucidated here.

Effect of parameter variations on model prediction

In Table 1, we used parameter values from previously published models (33,49), but the kinetic rate parameters vary widely for different cell and miRNA types (97–99). Following (100), we estimated $k_+ \sim 0.1 s^{-1}$ for miR-21 and $k_+ \sim 0.005 s^{-1}$ for miR-93, whereas measured value of $k_- \sim 0.0006 s^{-1}$ for mammalian cells. Further, for human cells, the mRNA degradation rate is about 10 times the protein degradation rate (101). Nevertheless, based on experimental studies, we varied the parameters near the realistic regime to check the robustness of our predictions (see "realistic parameter choices" in Materials and methods). If k_- decreases or k_+ increases (i.e., when the miRNA-mRNA association becomes stronger), the bimodality strength (κ) increases for the cases of no feedback and high feedback (see Fig. S6 *D–F* and *J–L*). However, the κ values are similar for the medium feedback. The variation in protein and miRNA-mRNA complex degradation rates did not alter κ values too much (Fig. S6 *A–C* and *G–I*). The variation in miRNA degradation rate (g_s) did not affect κ values too much for the no-feedback case, although κ quantitively depends on g_s with feedback (Fig. S6 *M–O*). Together, our qualitative predictions of observing bimodality near the threshold remain unchanged;

however, the bimodality strength and threshold locations depend on the exact parameter values (see Fig. S6).

We further checked if the alteration in protein bursting affects the bimodality. Previous studies (11,102) showed that the two-step protein production from a single gene (via transcription and translation) becomes bursty when the mRNA degradation rate (g_r) is much larger than the protein degradation rate (g_p). In this case, it is known that the burst size and burst frequency are controlled by the protein synthesis rate (k_p) and the protein degradation rate (g_p), respectively (11,102). We thus tuned the protein burst size and frequency by varying k_p or g_p by an order of magnitude. The time traces of protein numbers indeed showed that changing g_p (Fig. S7 *A*) or k_p (Fig. S7 *C*) affects the protein burst frequency or the burst size, respectively. Nevertheless, the bimodality strength was similar in both cases (Fig. S7 *B* and *D*), although the threshold locations changed noticeably. Thus, altering protein bursting does not change our qualitative prediction of observing bimodality near the threshold.

Limitation and future directions

In some parameter regimes, mean-field and moment-closure approximations used for our highly nonlinear system can yield significant errors in finding the threshold locations (see Figs. S8 and S9). Previous models on miRNA-based regulation (39,49,33) showed that a mean-field approximation works well to locate a very sharp transition. In our case, transitions are sharp only for no-feedback and high-feedback cases; otherwise, there is a shallow cross-over from low to high expression (see Fig. 2 *A*). Thus, the mean-field formula for the thresholds (k_r^{th} in Eq. 5) may hold at least in the limiting cases ($\beta = 0$ and high β).

Additionally, since the mRNA Fano factor peaks near the threshold (suggesting the system's high sensitivity near a transition), we may define the threshold as the peak position of the Fano factor. These peak positions determined from the *exact* Gillespie simulations are more rigorous definitions of thresholds (denoted by $k_{r|Gillespie}^{peak}$). We can also calculate the peak positions from the approximate SOMEs, denoted by $k_{r|SOME}^{peak}$ (see Section 6 in Supporting material). Thus, we can define two types of errors in estimating the thresholds corresponding to two different approximation methods: $\text{error}_1 = \left|k_{r|Gillespie}^{peak} - k_r^{th}\right| / k_{r|Gillespie}^{peak}$ (for mean field), and $\text{error}_2 = \left|k_{r|Gillespie}^{peak} - k_{r|SOME}^{peak}\right| / k_{r|Gillespie}^{peak}$ (for moment closure). We compared these errors in Fig. S9. As expected, both mean-field and SOME solutions worked for no-feedback and high-feedback limits (i.e., where cross-overs in mRNA mean are very sharp and the Fano factors are sharply peaked). In these cases, errors can be much less than $5\% - 10\%$ for SOME, and less than 20% for mean field, although the error is higher for medium feedback. The error also increases for low values of catalyticity parameter (α), i.e., when the miRNAs and mRNAs mostly do not co-degrade, and miRNAs often recycle back in the system. Overall, the moment closure is a better approximation in locating the actual threshold than the mean field.

We further compared our Gaussian moment closure with another approximation scheme, the Conditional Gaussian Moment Closure (103). Under this approximation, we solved the moment equations using a published package (104) in the parameter regime where our Gaussian approximation markedly differed from the Gillespie simulation (at a medium feedback strength). However, Conditional Gaussian Closure did not produce notably better results than our Gaussian closure (see Fig. S10).

Due to the complexity of our model, solving the highly nonlinear chemical Master equation (Eq. 1) would be an open problem. A recent theoretical paper advocated the linear mapping approximation (LMA), a helpful method by which bimolecular interactions can be substituted by zeroth or first-order reactions, reducing a nonlinear Master equation into a linear one and making the solution easier (105). Applying LMA in our model would be an interesting theoretical direction to pursue.

Our model focused on direct miRNA-mRNA interaction and neglected some other aspects of miRNA biogenesis. For instance, precursor miRNAs ultimately transform into mature miRNAs via several intermediate steps, and the precursor miRNAs also compete with mature miRNAs over the same target mRNA population (106). The miRNA maturation could lead to time delays that, combined with negative feedback, may generate interesting features such as stochastic oscillations in expression (107,108). Moreover, during the miRNA maturation process, a single miRNA locus can generate a series of sequences, typically known as isomiRs (109,110), which can bind with the same target mRNAs. Such competitive dynamics of precursor miRNAs or isomiRs with matured mRNAs are still unexplored. Note that such competition between several kinds of noncoding RNA sequences sharing a common target mRNA pool is conceptually different from the ceRNA network, where several target mRNAs share the same miRNAs.

Another aspect ignored in our model is that target mRNAs can have multiple miRNA binding sites, leading to additional roles in gene regulation, as shown in experiments (50,111). Recent theoretical and experimental studies (112,113) also found that multi-site miRNA binding can generate bimodality and oscillation even without a feedback loop. Thus, comparing the transcriptional feedback-driven bimodality and the multiple binding site-driven bimodality in miRNA-based motifs can be important for future work. Also, by extending our model, it can be interesting to explore how a two-state miRNA-producing gene regulates its own TFs synthesized from another two-state promoter.

Several experimental techniques, including synthetic design of genetic circuits, fluorescent microscopy, and

flow cytometry, have been used in single-cell experiments and bulk expression measurements related to miRNA-dependent gene expression (39,45,67). Such experiments can provide accurate quantitative testing of theoretical predictions as described in this paper. Our results further suggests that cells may chemically control many processes involving miRNAs, such as the catalytic mode of repression, miRNA-mRNA association rate, and the feedback strength to tune the gene expression noise. For instance, experimental studies have shown that the phosphorylation of RISC proteins can control the mature miRNA binding to target mRNAs (114), creating a regulating knob for the effective miRNA-mRNA association rate. Our study revealed the key tuning parameters that may be connected with experiments to know how expression diversity is regulated in a miRNA-based negative-feedback loop.

MATERIALS AND METHODS

We simulated the model using the Gillespie algorithm (86). The codes were written in FORTRAN90, and they are freely available in the following link: https://github.com/PhyBi/miRNA-negative-feedback.

Realistic parameter choices

Although we used parameter values (in Table 1) from previously published models (33,49), there are large variations in the kinetic rate parameters for different cell and miRNA types and different target genes (97–99). Nevertheless, based on experimental studies, we present below a discussion on choosing realistic kinetic rates, which we used to check the robustness of our predictions.

mRNA-miRNA association and dissociation rates (k_+ and k_-)

Wee et al. (100) have measured the dissociation constant (K_d) for the miRNA-mRNA complex corresponding to mouse and fly Ago2 proteins (these guide miRNAs to silence target mRNAs). The K_d values ranged from 13 to 26pM. The authors also separately measured the miRNA-mRNA dissociation rates (k_-). Using these measurements, the authors estimated the complex formation rate ($k_{on} = k_-/K_d$). Note that the measured K_d, k_{on}, and k_- values are expressed in units of pM, $M^{-1}s^{-1}$, and s^{-1}, respectively (see Fig. 7 in Ref. (100)). To understand these units, we note $k_{on}[s][m] = k_-[c]$ at kinetic equilibrium (following the mass-action principle), where $[s]$, $[m]$, and $[c]$ are equilibrium concentrations of miRNAs, mRNAs, and complexes. Thus, we can estimate the miRNA-mRNA association rate (k_+ in s^{-1}) used in our stochastic framework as $k_+ = k_{on}[s]$. Here, $[s]$ can be taken as the cellular concentration of miRNAs. Using this relation, we can estimate k_+ values from the measured k_{on} values, namely $k_{on} = 0.36 \times 10^8 M^{-1}s^{-1}$ (corresponding to 13 pM K_d) and $k_{on} = 0.2 \times 10^8 M^{-1}s^{-1}$ (corresponding to 26 pM K_d). Moreover, the concentration of highly abundant miRNAs such as miR-21 in HeLa cells is 4 nM, whereas some low-abundant miRNAs such as miR-93 have a concentration of 140 pM (100). Thus, we estimated $k_+ = 0.08s^{-1}\&0.1s^{-1}$ for miR-21 (corresponding to 26 and 13 pM K_d, respectively) and $k_+ = 0.002s^{-1}\&0.005s^{-1}$ for miR-93. As shown in Table 1, we thus varied k_+ from 0.001 to 0.1.

The authors also separately measured the miRNA-mRNA dissociation rates (k_-), given by $k_- = 0.00077s^{-1}\&0.00046s^{-1}$ for mouse Ago2 and $k_- = 0.045s^{-1}$ and $0.088s^{-1}$ for fly Ago2. This gives a mean of $k_- = 0.0006s^{-1}$ for the mouse and $0.066s^{-1}$ for the fly. In Table 1, we used $k_- = 0.0036s^{-1}$, which is an order of magnitude higher than mouse Ago2 but lower than fly Ago 2. In Fig. S6, we used $k_- = 0.0006s^{-1}$ (corresponding to the mammalian value) to check the effect of realistic parameters.

miRNA degradation rate (g_s)

It was shown that the median half-life of miRNAs (for most abundant miR strands that are bound by Ago proteins) is about 11.4 h (115,116). Thus, the miRNA degradation rate (g_s) can be given by $g_s = ln\,2/11.4h = 0.000017s^{-1}$. This value is an order of magnitude lower than the value used in Table 1. We nevertheless varied g_s and found that our qualitative observation of bimodality near the threshold remains unchanged, although the bimodality strength depends on the values of g_s.

Degradation rates of target mRNAs and proteins (g_r and g_p)

It was known that mRNA degradation rates are an order of magnitude faster than protein degradation rates in eukaryotes (see Table 1 in Ref. (101)). Following Jia (101), we estimated that the protein degradation rates of budding yeast, fission yeast, and human cells are similar, about $g_p \sim 0.00002/s$. On the other hand, the mRNA degradation rates for budding yeast, fission yeast, and human cells are $0.0002/s$, $0.0004/s$, and $0.0006/s$, respectively; i.e., $g_r = 0.0004/s$ on average for these eukaryotic cells, consistent with Table 1. Thus, for human cells, $g_r \sim 10g_p$ (101), and we maintained this relation for choosing a realistic parameter set.

Based on the above discussion, in Fig. S6, we used a realistic parameter set given by $g_r = 0.0004s^{-1}$, $g_p = 0.00002s^{-1}$, $g_s = 0.000017s^{-1}$, $k_+ = 0.1s^{-1}$, and $k_- = 0.0006s^{-1}$.

SUPPORTING MATERIAL

Supporting material can be found online at https://doi.org/10.1016/j.bpj.2023.09.019.

AUTHOR CONTRIBUTIONS

D.D. and M.K.J. designed the research and supervised the study. R.A. and A.R. carried out all simulations and analyzed the data. D.D. and R.A. wrote the manuscript with input from A.R. and M.K.J.

ACKNOWLEDGMENTS

D.D. thanks DST-SERB, Government of India (project no. SRG/2019/001068) for the financial support. R.A. thanks CSIR, India for his fellowship (award no. 09/921(0282)/2019-EMR-I).

DECLARATION OF INTERESTS

The authors declare no competing interests.

REFERENCES

1. Watson, J. D., T. A. Baker, …, R. M. Losick. 2004. Molecular Biology of the Gene. Pearson/CSHLpress.
2. Raser, J. M., and E. K. O'Shea. 2005. Noise in Gene Expression: Origins, Consequences, and Control. *Science.* 309:2010–2013. https://doi.org/10.1126/science.1105891.

3. Kaern, M., T. C. Elston, …, J. J. Collins. 2005. Stochasticity in gene expression: from theories to phenotypes. *Nat. Rev. Genet.* 6:451–464.
4. Kaufmann, B. B., and A. van Oudenaarden. 2007. Stochastic gene expression: from single molecules to the proteome. *Curr. Opin. Genet. Dev.* 17:107–112.
5. Sanchez, A., S. Choubey, and J. Kondev. 2013. Regulation of noise in gene expression. *Annu. Rev. Biophys.* 42:469–491.
6. Munsky, B., G. Neuert, and A. van Oudenaarden. 2012. Using Gene Expression Noise to Understand Gene Regulation. *Science.* 336:183–187. https://doi.org/10.1126/science.1216379.
7. Thattai, M., and A. Van Oudenaarden. 2001. Intrinsic noise in gene regulatory networks. *Proc. Natl. Acad. Sci. USA.* 98:8614–8619.
8. Elowitz, M. B., A. J. Levine, …, P. S. Swain. 2002. Stochastic gene expression in a single cell. *Science.* 297:1183–1186.
9. Raj, A., and A. Van Oudenaarden. 2008. Nature, nurture, or chance: stochastic gene expression and its consequences. *Cell.* 135:216–226.
10. Sanchez, A., and I. Golding. 2013. Genetic determinants and cellular constraints in noisy gene expression. *Science.* 342:1188–1193.
11. Shahrezaei, V., and P. S. Swain. 2008. Analytical distributions for stochastic gene expression. *Proc. Natl. Acad. Sci. USA.* 105:17256–17261.
12. Sanchez, A., S. Choubey, and J. Kondev. 2013. Stochastic models of transcription: From single molecules to single cells. *Methods.* 62:13–25.
13. Sanchez, A., H. G. Garcia, …, J. Kondev. 2011. Effect of promoter architecture on the cell-to-cell variability in gene expression. *PLoS Comput. Biol.* 7, e1001100.
14. Sánchez, A., and J. Kondev. 2008. Transcriptional control of noise in gene expression. *Proc. Natl. Acad. Sci. USA.* 105:5081–5086.
15. Das, D., S. Dey, …, S. Choubey. 2017. Effect of transcription factor resource sharing on gene expression noise. *PLoS Comput. Biol.* 13:10054911–e1005520. https://doi.org/10.1371/journal.pcbi.1005491.
16. Dey, S., M. Soltani, and A. Singh. 2020. Enhancement of gene expression noise from transcription factor binding to genomic decoy sites. *Sci. Rep.* 10:9126.
17. Jones, D. L., R. C. Brewster, and R. Phillips. 2014. Promoter architecture dictates cell-to-cell variability in gene expression. *Science.* 346:1533–1536.
18. Choi, P. J., L. Cai, …, X. S. Xie. 2008. A stochastic single-molecule event triggers phenotype switching of a bacterial cell. *Science.* 322:442–446.
19. Ferguson, M. L., D. Le Coq, …, C. A. Royer. 2012. Reconciling molecular regulatory mechanisms with noise patterns of bacterial metabolic promoters in induced and repressed states. *Proc. Natl. Acad. Sci. USA.* 109:155–160.
20. Taniguchi, Y., P. J. Choi, …, X. S. Xie. 2010. Quantifying E. coli proteome and transcriptome with single-molecule sensitivity in single cells. *Science.* 329:533–538.
21. Raj, A., C. S. Peskin, …, S. Tyagi. 2006. Stochastic mRNA synthesis in mammalian cells. *PLoS Biol.* 4:e309.
22. Grönlund, A., P. Lötstedt, and J. Elf. 2013. Transcription factor binding kinetics constrain noise suppression via negative feedback. *Nat. Commun.* 4:1864.
23. Maamar, H., A. Raj, and D. Dubnau. 2007. Noise in gene expression determines cell fate in Bacillus subtilis. *Science.* 317:526–529.
24. Kussell, E., and S. Leibler. 2005. Phenotypic Diversity, Population Growth, and Information in Fluctuating Environments. *Science.* 309:2075–2078. https://doi.org/10.1126/science.1114383.
25. Blake, W. J., G. Balázsi, …, J. J. Collins. 2006. Phenotypic consequences of promoter-mediated transcriptional noise. *Mol. Cell.* 24:853–865.
26. Thattai, M., and A. Van Oudenaarden. 2004. Stochastic gene expression in fluctuating environments. *Genetics.* 167:523–530.
27. Gottesman, S. 2004. The small RNA regulators of Escherichia coli: roles and mechanisms. *Annu. Rev. Microbiol.* 58:303–328.
28. Gottesman, S. 2005. Micros for microbes: non-coding regulatory RNAs in bacteria. *Trends Genet.* 21:399–404.
29. Gottesman, S., C. McCullen, …, D. FitzGerald. 2006. Small RNA regulators and the bacterial response to stress. *In* Cold Spring Harbor Symposia on Quantitative Biology Cold Spring Harbor Laboratory Press, pp. 1–11.
30. Levine, E., Z. Zhang, …, T. Hwa. 2007. Quantitative characteristics of gene regulation by small RNA. *PLoS Biol.* 5:e229.
31. Mitarai, N., J.-A. M. Benjamin, …, K. Sneppen. 2009. Dynamic features of gene expression control by small regulatory RNAs. *Proc. Natl. Acad. Sci. USA.* 106:10655–10659. https://doi.org/10.1073/pnas.0901466106.
32. Kumar, N., K. Zarringhalam, and R. V. Kulkarni. 2018. Stochastic Modeling of Gene Regulation by Noncoding Small RNAs in the Strong Interaction Limit. *Biophys. J.* 114:2530–2539.
33. Bosia, C., A. Pagnani, and R. Zecchina. 2013. Modelling competing endogenous RNA networks. *PLoS One.* 8, e66609.
34. Li, X., J. J. Cassidy, …, R. W. Carthew. 2009. A microRNA imparts robustness against environmental fluctuation during development. *Cell.* 137:273–282.
35. Li, Y., F. Wang, …, F.-B. Gao. 2006. MicroRNA-9a ensures the precise specification of sensory organ precursors in Drosophila. *Genes Dev.* 20:2793–2805.
36. Lamouille, S., D. Subramanyam, …, R. Derynck. 2013. Regulation of epithelial–mesenchymal and mesenchymal–epithelial transitions by microRNAs. *Curr. Opin. Cell Biol.* 25:200–207.
37. Caldas, C., and J. D. Brenton. 2005. Sizing up miRNAs as cancer genes. *Nat. Med.* 11:712–714.
38. Shenouda, S. K., and S. K. Alahari. 2009. MicroRNA function in cancer: oncogene or a tumor suppressor? *Cancer Metastasis Rev.* 28:369–378.
39. Mukherji, S., M. S. Ebert, …, A. van Oudenaarden. 2011. MicroRNAs can generate thresholds in target gene expression. *Nat. Genet.* 43:854–859.
40. Hutvágner, G., and P. D. Zamore. 2002. A microRNA in a multiple-turnover RNAi enzyme complex. *Science.* 297:2056–2060.
41. Arvey, A., E. Larsson, …, D. S. Marks. 2010. Target mRNA abundance dilutes microRNA and siRNA activity. *Mol. Syst. Biol.* 6:363.
42. Kai, Z. S., and A. E. Pasquinelli. 2010. MicroRNA assassins: factors that regulate the disappearance of miRNAs. *Nat. Struct. Mol. Biol.* 17:5–10.
43. Pillai, R. S., S. N. Bhattacharyya, …, W. Filipowicz. 2005. Inhibition of translational initiation by Let-7 MicroRNA in human cells. *Science.* 309:1573–1576.
44. Bartel, D. P. 2004. MicroRNAs: genomics, biogenesis, mechanism, and function. *Cell.* 116:281–297.
45. Bosia, C., F. Sgrò, …, R. Zecchina. 2017. RNAs competin g for microRNAs mutually influence their fluctuations in a highly non-linear microRNA-dependent manner in single cells. *Genome Biol.* 18:1–14.
46. Del Giudice, M., S. Bo, …, C. Bosia. 2018. On the role of extrinsic noise in microRNA-mediated bimodal gene expression. *PLoS Comput. Biol.* 14, e1006063.
47. Waters, L. S., and G. Storz. 2009. Regulatory RNAs in bacteria. *Cell.* 136:615–628.
48. Gottesman, S., and G. Storz. 2011. Bacterial small RNA regulators: versatile roles and rapidly evolving variations. *Cold Spring Harbor Perspect. Biol.* 3:a003798.
49. Noorbakhsh, J., A. H. Lang, and P. Mehta. 2013. Intrinsic noise of microRNA-regulated genes and the ceRNA hypothesis. *PLoS One.* 8, e72676.
50. Schmiedel, J. M., S. L. Klemm, …, A. van Oudenaarden. 2015. MicroRNA control of protein expression noise. *Science.* 348:128–132.

51. Bose, I., and S. Ghosh. 2012. Origins of binary gene expression in post-transcriptional regulation by microRNAs. *Eur. Phys. J. E Soft Matter.* 35:102–108.
52. Hao, Y., L. Xu, and H. Shi. 2011. Theoretical analysis of catalytic-sRNA-mediated gene silencing. *J. Mol. Biol.* 406:195–204.
53. Sumazin, P., X. Yang, …, A. Califano. 2011. An extensive microRNA-mediated network of RNA-RNA interactions regulates established oncogenic pathways in glioblastoma. *Cell.* 147:370–381.
54. Ala, U., F. A. Karreth, …, P. P. Pandolfi. 2013. Integrated transcriptional and competitive endogenous RNA networks are cross-regulated in permissive molecular environments. *Proc. Natl. Acad. Sci. USA.* 110:7154–7159.
55. Figliuzzi, M., E. Marinari, and A. De Martino. 2013. MicroRNAs as a Selective Channel of Communication between Competing RNAs: a Steady-State Theory. *Biophys. J.* 104:1203–1213. https://www.sciencedirect.com/science/article/pii/S0006349513000829.
56. Levine, E., M. Huang, …, T. Hwa. 2008. On Noise and Silence in Small RNA Regulation. matisse.ucsd.edu/hwa/pub/sRNA-noise.pdf. Preprint.
57. Tsang, J., J. Zhu, and A. van Oudenaarden. 2007. MicroRNA-mediated feedback and feedforward loops are recurrent network motifs in mammals. *Mol. Cell.* 26:753–767.
58. Emmrich, S., and B. M. Pützer. 2010. Checks and balances: E2F—microRNA crosstalk in cancer control. *Cell Cycle.* 9:2555–2567.
59. Concepcion, C. P., C. Bonetti, and A. Ventura. 2012. The miR-17-92 family of microRNA clusters in development and disease. *Cancer J.* 18:262–267.
60. Aguda, B. D., Y. Kim, …, C. B. Marsh. 2008. MicroRNA regulation of a cancer network: consequences of the feedback loops involving miR-17-92, E2F, and Myc. *Proc. Natl. Acad. Sci. USA.* 105:19678–19683.
61. Wong, J. J.-L., A. Y. M. Au, …, W. Ritchie. 2016. RBM3 regulates temperature sensitive miR-142–5p and miR-143 (thermomiRs), which target immune genes and control fever. *Nucleic Acids Res.* 44:2888–2897.
62. Fox, Z., and A. Singh. 2014. Stochastic analysis of protein-mediated and microRNA-mediated feedback circuits in HIV. *IFAC Proc. Vol.* 47:1146–1151.
63. Lu, M., M. K. Jolly, …, E. Ben-Jacob. 2013. MicroRNA-based regulation of epithelial–hybrid–mesenchymal fate determination. *Proc. Natl. Acad. Sci. USA.* 110:18144–18149.
64. Jolly, M. K., M. Boareto, …, H. Levine. 2015. Implications of the hybrid epithelial/mesenchymal phenotype in metastasis. *Front. Oncol.* 5:155.
65. Kim, J., K. Inoue, …, A. Abeliovich. 2007. A MicroRNA Feedback Circuit in Midbrain Dopamine Neurons. *Science.* 317:1220–1224. https://doi.org/10.1126/science.1140481.
66. Lai, X., O. Wolkenhauer, and J. Vera. 2016. Understanding microRNA-mediated gene regulatory networks through mathematical modelling. *Nucleic Acids Res.* 44:6019–6035.
67. Siciliano, V., I. Garzilli, …, D. Di Bernardo. 2013. MiRNAs confer phenotypic robustness to gene networks by suppressing biological noise. *Nat. Commun.* 4:2364–2367.
68. Bosia, C., M. Osella, …, M. Caselle. 2012. Gene autoregulation via intronic microRNAs and its functions. *BMC Syst. Biol.* 6:131–216.
69. Zhou, P., S. Cai, …, R. Wang. 2012. Mechanisms generating bistability and oscillations in microRNA-mediated motifs. *Phys. Rev.* 85, 041916.
70. Wang, S., and S. Raghavachari. 2011. Quantifying negative feedback regulation by micro-RNAs. *Phys. Biol.* 8, 055002.
71. Ferrell, J. E., Jr. 2002. Self-perpetuating states in signal transduction: positive feedback, double-negative feedback and bistability. *Curr. Opin. Cell Biol.* 14:140–148.
72. Shen-Orr, S. S., R. Milo, …, U. Alon. 2002. Network motifs in the transcriptional regulation network of Escherichia coli. *Nat. Genet.* 31:64–68.
73. Takahashi, J. S. 2017. Transcriptional architecture of the mammalian circadian clock. *Nat. Rev. Genet.* 18:164–179.
74. Smits, W. K., O. P. Kuipers, and J.-W. Veening. 2006. Phenotypic variation in bacteria: the role of feedback regulation. *Nat. Rev. Microbiol.* 4:259–271.
75. Pomerening, J. R. 2008. Uncovering mechanisms of bistability in biological systems. *Curr. Opin. Biotechnol.* 19:381–388.
76. Karmakar, R., and I. Bose. 2007. Positive feedback, stochasticity and genetic competence. *Phys. Biol.* 4:29–37.
77. Holehouse, J., Z. Cao, and R. Grima. 2020. Stochastic modeling of autoregulatory genetic feedback loops: A review and comparative study. *Biophys. J.* 118:1517–1525.
78. Hasty, J., J. Pradines, …, J. J. Collins. 2000. Noise-based switches and amplifiers for gene expression. *Proc. Natl. Acad. Sci. USA.* 97:2075–2080.
79. Nevozhay, D., R. M. Adams, …, G. Balázsi. 2009. Negative autoregulation linearizes the dose–response and suppresses the heterogeneity of gene expression. *Proc. Natl. Acad. Sci. USA.* 106:5123–5128.
80. Dublanche, Y., K. Michalodimitrakis, …, L. Serrano. 2006. Noise in transcription negative feedback loops: simulation and experimental analysis. *Mol. Syst. Biol.* 2:41. https://doi.org/10.1038/msb4100081.
81. Simpson, M. L., C. D. Cox, and G. S. Sayler. 2003. Frequency domain analysis of noise in autoregulated gene circuits. *Proc. Natl. Acad. Sci. USA.* 100:4551–4556.
82. Singh, A., and J. P. Hespanha. 2009. Optimal feedback strength for noise suppression in autoregulatory gene networks. *Biophys. J.* 96:4013–4023.
83. Marquez-Lago, T. T., and J. Stelling. 2010. Counter-intuitive stochastic behavior of simple gene circuits with negative feedback. *Biophys. J.* 98:1742–1750.
84. Liu, P., Z. Yuan, …, T. Zhou. 2016. Decomposition and tunability of expression noise in the presence of coupled feedbacks. *Chaos.* 26, 043108.
85. Jia, C., P. Xie, …, M. Q. Zhang. 2017. Stochastic fluctuations can reveal the feedback signs of gene regulatory networks at the single-molecule level. *Sci. Rep.* 7, 16037.
86. Gillespie, D. T. 1976. A general method for numerically simulating the stochastic time evolution of coupled chemical reactions. *J. Comput. Phys.* 22:403–434.
87. Dobrzyński, M., and F. J. Bruggeman. 2009. Elongation dynamics shape bursty transcription and translation. *Proc. Natl. Acad. Sci. USA.* 106:2583–2588.
88. Bartman, C. R., S. C. Hsu, …, G. A. Blobel. 2016. Enhancer regulation of transcriptional bursting parameters revealed by forced chromatin looping. *Mol. Cell.* 62:237–247.
89. Jia, C., and R. Grima. 2020. Dynamical phase diagram of an autoregulating gene in fast switching conditions. *J. Chem. Phys.* 152:174110.
90. Chau, Y.-F. C., C.-K. Wang, …, N. Y. Voo. 2017. Simultaneous realization of high sensing sensitivity and tunability in plasmonic nanostructures arrays. *Sci. Rep.* 7, 16817.
91. Jia, C., L. Y. Wang, …, M. Q. Zhang. 2019. Single-cell stochastic gene expression kinetics with coupled positive-plus-negative feedback. *Phys. Rev. E.* 100, 052406.
92. Jia, C., and R. Grima. 2020. Small protein number effects in stochastic models of autoregulated bursty gene expression. *J. Chem. Phys.* 152:084115.
93. Ghosh, S., S. Banerjee, and I. Bose. 2012. Emergent bistability: Effects of additive and multiplicative noise. *Eur. Phys. J. E Soft Matter.* 35:11–14.
94. Pájaro, M., I. Otero-Muras, …, A. A. Alonso. 2019. Transient hysteresis and inherent stochasticity in gene regulatory networks. *Nat. Commun.* 10:4581.
95. Lee, J., and J. Lee. 2018. Quantitative analysis of a transient dynamics of a gene regulatory network. *Phys. Rev. E.* 98, 062404.

96. Sylvestre, Y., V. De Guire, …, P. Chartrand. 2007. An E2F/miR-20a autoregulatory feedback loop. *J. Biol. Chem.* 282:2135–2143.

97. Dalmay, T. 2013. Mechanism of miRNA-mediated repression of mRNA translation. *Essays Biochem.* 54:29–38.

98. Jonas, S., and E. Izaurralde. 2015. Towards a molecular understanding of microRNA-mediated gene silencing. *Nat. Rev. Genet.* 16:421–433.

99. Jia, C., and R. Grima. 2021. Frequency domain analysis of fluctuations of mRNA and protein copy numbers within a cell lineage: theory and experimental validation. *Phys. Rev. X.* 11, 021032.

100. Wee, L. M., C. F. Flores-Jasso, …, P. D. Zamore. 2012. Argonaute divides its RNA guide into domains with distinct functions and RNA-binding properties. *Cell.* 151:1055–1067.

101. Jia, C. 2017. Simplification of Markov chains with infinite state space and the mathematical theory of random gene expression bursts. *Phys. Rev. E.* 96, 032402.

102. Friedman, N., L. Cai, and X. S. Xie. 2006. Linking stochastic dynamics to population distribution: an analytical framework of gene expression. *Phys. Rev. Lett.* 97, 168302.

103. Soltani, M., C. A. Vargas-Garcia, and A. Singh. 2015. Conditional moment closure schemes for studying stochastic dynamics of genetic circuits. *IEEE Trans. Biomed. Circuits Syst.* 9:518–526.

104. Sukys, A., and R. Grima. 2021. MomentClosure. jl: automated moment closure approximations in Julia. *Bioinformatics.* 38:289–290.

105. Cao, Z., and R. Grima. 2018. Linear mapping approximation of gene regulatory networks with stochastic dynamics. *Nat. Commun.* 9:3305–3315.

106. Roy-Chaudhuri, B., P. N. Valdmanis, …, M. A. Kay. 2014. Regulation of microRNA-mediated gene silencing by microRNA precursors. *Nat. Struct. Mol. Biol.* 21:825–832.

107. Barrio, M., K. Burrage, …, T. Tian. 2006. Oscillatory Regulation of Hes1: Discrete Stochastic Delay Modelling and Simulation. *PLoS Comput. Biol.* 2:1177–e214. https://doi.org/10.1371/journal.pcbi.0020117.

108. Bratsun, D., D. Volfson, …, J. Hasty. 2005. Delay-induced stochastic oscillations in gene regulation. *Proc. Natl. Acad. Sci. USA.* 102:14593–14598. https://doi.org/10.1073/pnas.0503858102.

109. Neilsen, C. T., G. J. Goodall, and C. P. Bracken. 2012. IsomiRs–the overlooked repertoire in the dynamic microRNAome. *Trends Genet.* 28:544–549.

110. Guo, L., and F. Chen. 2014. A challenge for miRNA: multiple isomiRs in miRNAomics. *Gene.* 544:1–7.

111. Wei, L., S. Li, …, X. Wang. 2021. Characterizing microRNA-mediated modulation of gene expression noise and its effect on synthetic gene circuits. *Cell Rep.* 36:109573.

112. Nordick, B., P. Y. Yu, …, T. Hong. 2022. Nonmodular oscillator and switch based on RNA decay drive regeneration of multimodal gene expression. *Nucleic Acids Res.* 50:3693–3708.

113. Li, C.-J., E. S. Liau, …, T. Hong. 2021. MicroRNA governs bistable cell differentiation and lineage segregation via a noncanonical feedback. *Mol. Syst. Biol.* 17:e9945.

114. Rüdel, S., Y. Wang, …, G. Meister. 2010. Phosphorylation of human Argonaute proteins affects small RNA binding. *Nucleic Acids Res.* 39:2330–2343. https://doi.org/10.1093/nar/gkq1032.

115. Zlotorynski, E. 2019. Insights into the kinetics of microRNA biogenesis and turnover. *Nat. Rev. Mol. Cell Biol.* 20:511.

116. Reichholf, B., V. A. Herzog, …, S. L. Ameres. 2019. Time-resolved small RNA sequencing unravels the molecular principles of microRNA homeostasis. *Mol. Cell.* 75:756–768.e7.